CHALMERS

SIMULATION OF GAS DISPERSION IN ROAD TUNNEL WITH TRAFFIC

Computational Fluid Dynamics Simulation using FLUENT and In-house TU Delft codes

Master of Science Thesis [Innovative and Sustainable Chemical Engineering]

MUHAMMAD MUZAMAL

Department of Chemical and Biological Engineering
Chemical Reaction Engineering
CHALMERS UNIVERSITY OF TECHNOLOGY
Gothenburg, Sweden, 2011

SIMULATION OF GAS DISPERSION IN ROAD TUNNEL WITH TRAFFIC

Computational Fluid Dynamics Simulation using FLUENT and In-house TU Delft codes

MUHAMMAD MUZAMAL

Supervised by

Prof. Dirk Roekaerts
Department of Multi-Scale Physics
Faculty of Applied Sciences
Delft University of Technology

Prof. Bengt Andersson
Department of Chemical and Biological Engineering
Chemical Reaction Engineering
Chalmers University of Technology

Department of Chemical and Biological Engineering
CHALMERS UNIVERSITY OF TECHNOLOGY
Gothenburg, Sweden 2011

Department of Multi-scale Physics
DELFT UNIVERSITY OF TECHNOLOGY
Delft, Netherlands 2011

Defense, Security and Safety
TNO
Utrecht, Netherlands 2011

ACKNOWLEDGMENT

I would like to thank Professor Dr. Dirk Roekaerts for letting me work on this project and guiding me nicely throughout the project. It was a great opportunity for me. I learned precious knowledge while working with extremely talented team. I would also thank Dr. Sasa Kenjeres for his direction, assistance, and guidance. Special thanks to Professor Dr. Bengt Andersson, whose recommendations and suggestions have been invaluable for this project. I also wish to thank Michael Stoellinger, who have helped me lot. His company was always nice and beneficial. Thanks are also due to my student colleagues, Mike and Sinta who helped me in many ways. Finally, words alone cannot express the thanks I owe to, my brothers. Their prayers made this all happened.

Thank you all!

ABSTRACT

The transportation of flammable gas like LPG is banned, through many road tunnels, in Netherlands. In the case of accident, this flammable gas can make flammable mixture in tunnel and cause serious explosion. An experimental setup mimicking a road tunnel has been built at TU Delft. It is a small scale tunnel with obstacles. These obstacles represent the cars from traffic jam in a tunnel. Water (with $\rho = 998\ kg/m^3$ and velocity $U_\infty = 0.15\ m/s$) is used as main stream in the experimental setup representing the air and saline solution (with $\rho_j = 1060\ kg/m^3$ and velocity $U_j = 2.3\ m/s$) represents the flammable gas. The salt water is injected at right angle through the square opening in the bottom, forming jet in the cross-flow.

In this study CFD modeling is performed to simulate the experimental setup. Different turbulence models are tested. These models are validated through the experimental results. Simulation is performed using commercial CFD software ANSYS FLUENT and using In-house TU Delft codes. When using FLUENT, Reynolds stress turbulence model is used to perform simulation. On the other hand Standard *k-ε* and modified *k-ε* models are tested through In-house codes. The results of the simulation are being validated through the measurements. It has been identified that Reynolds stress model shows close agreement with experimental results of velocities. However the values of turbulent kinetic energy and Reynolds stress show some disagreement with measurements. The scalar dispersion has been analyzed with Reynolds stress model. Because the In-house code require some modifications which have been suggested during this study. Simulation performed with Standard *k-ε* and modified *k-ε* models using In-house codes will serve as bases for further studies.

The simulation is then generalized to transportation of other fuels like H_2 gas. The simulation is performed with water (with $\rho = 998\ kg/m^3$ and velocity $U_\infty = 0.15\ m/s$) as main stream representing air and light liquid (with $\rho_j = 927\ kg/m^3$ and velocity $U_j = 2.3\ m/s$) representing H_2 as jet. The dispersion of gas is being studies and it is analyzed that density difference has significant effect on scalar dispersion. Finally the simulation is performed with low jet velocity ($U_j = 1.15\ m/s$) to identify the importance of jet-to-cross-flow velocity ratio.

Table of Contents

CHAPTER 1

INTRODUCTION

In this chapter a brief overview of the project is presented. Purpose and objectives of the project are explained in the introduction. Then literature study of different research papers is included. In these research papers, study related to current project was done. It is explained how this study contributes to research on jet in cross-flow. An experimental setup was built at TU Delft. The simulation in this study is validated through the results of that experiment. Detailed overview of the experimental setup is presented in the end.

1.1. INTRODUCTION

The transportation of Liquefied Petroleum gas (LPG) and other flammable gases is not allowed through many road tunnels in Netherlands due to risk of explosion. Leakage of flammable gases inside a tunnel can form a flammable mixture which has high chances of explosion.

Figure 1.1: Road tunnel with two lanes

Similar catastrophic incident took place on 18, March 1996, when a truck carrying LPG had an accident in the road tunnel near Palermo, Italy. The truck was involved in a car crash that gave rise to the release of propane gas through a crack that formed on the top of the vessel. The ignition of the gas cloud, that was created, caused serious disaster and 25 injuries. The report presented by Ciambelli, Bucciero, and Maremonti (1997) explains the risk involved in transportation of flammable gas like LPG through road tunnel. The report includes the case history of a BLEVE of a tank truck transporting LPG that occurred in a road tunnel near Palermo, Italy.

This project ‘’Simulation of gas dispersion in road tunnel’’ is a step to investigate how gas will be dispersed in case of accidental release inside a road tunnel and how much, different models, are successful in predicting the gas dispersion and velocity fields inside the tunnel. This study is beneficial for the improvement of tunnel’s safety.

Different attempts have been made to simulate gas dispersion in road tunnel using different computational fluid dynamics (CFD) techniques. Simulations using Ventunnel codes and CFX were performed and results are available (Trijssenaar-Buhre, Van der Walle and Wijnant-Timmerman 2009). This project is carried out to test different CFD models. The results of these models are validated through measurements.

An experimental setup mimicking a road tunnel has been built in TU Delft. It is a small scale tunnel with obstacles. The obstacles represent the cars from traffic jam in a tunnel. Water is used as main stream in the experimental setup representing the air and salt water solution represents flammable gas. A number of experiments have been carried out in which the dispersion of a heavy fluid in the small scale tunnel with obstacles is studied. The experimental database consists of velocity fields measured using PIV and concentration fields using LIF of a dye added to the salt water. The available experimental data set serves as a basis for validation of CFD models.

The heavy fluid is injected into the cross-flow through a square opening in the floor of the tunnel. This specific study in which a jet is injected into a cross flow stream lies in the category of 'jet in cross flow'. Much research has already being carried out on this topic. However this study differs in the sense that the cross-flow is affected by the presence of obstacles. Also CFD simulation is performed using the approaches which have not been tested before.

In the first part of the project, simulation of the experimental scale tunnel is performed with Reynolds Stress turbulence model using commercial CFD software ANSYS FLUENT. Different improvements for the simulations are suggested to obtain better accuracy of the results. The results are then validated through available measurements. The experimental results are comprises of U velocity, V velocity, Turbulence kinetic energy and uv Reynolds Stress. Then simulation using In-house Delft code is performed. In this part standard k-ε and modified k-ε models are tested. The results from these models are then compared with the results obtained from Reynolds stress model and measurements. If a model can predict velocity fields and turbulence kinetic energy with good accuracy, it is supposed that it can nicely predict the dispersion of gas as well. Finally the interpretation of the CFD simulations is generalised to other cases. In these cases the importance of velocity ratio and density ratio are identified.

1.2. Literature Review

The Study of literature showed that plenty of research has already been carried out in this field of study. This specific study in which a jet is injected into a cross-flow stream lies in the category of 'jet in cross flow' (JICF) (Plesniak 2005). So far in the research different scenarios of JICF have been studied including experimental and numerical investigations. Influence of important variables on JICF has been studied. Few research papers emphasized on shape of jet and its different regimes. Comparison of rectangular and circular jet in cross flow was also part of same study. Research showed that no systematic and complete study is available in which JICF is simulated using different turbulence models. This specific study differs from previous studies on JICF in the sense that it includes obstacles in the flow and numerical simulation is done using turbulence models in FLUENT and In-house Delft codes.

In the report of Ciambelli, Bucciero and Maremonti (1997) the CFD modeling is performed using the codes called AutoReags, developed by TNO (Netherlands) and Century Dynamics Ltd (UK). In the report modeling of BLEVE was done. The model produced a good prediction of the failure time. It was concluded that the characteristic time of BLEVE (boiling liquid expanding vapor explosion) in confined areas such as road tunnel are significantly shorter than those in open environment. This means that the scenario of accident, of truck carrying flammable gas, inside tunnel is more critical than in open environment.

JICF is often used in industrial applications to promote scalar mixing and a lot of research is done to improve scalar transport in cross-flow. In the experimental investigation carried out by Plesniak (2005) a confined rectangular jet in a cross-flow was considered. The experiments were performed by varying important parameters like velocity ratio, downstream distance and injection angles. It was found that the jet has three main regions. These are Horseshoe vortex (HSV), wake vortices and Counter rotating vortex pair (CRVP). These regions were found to be very important for scalar mixing especially CRVP. These regions can be seen in Figure 1.2. Another important effect found was asymmetry in jet shape even though cross flow and jet injection was symmetric. It was concluded that this asymmetry might be caused by non-uniform amplification of the fundamental mechanism which produces CRVP.

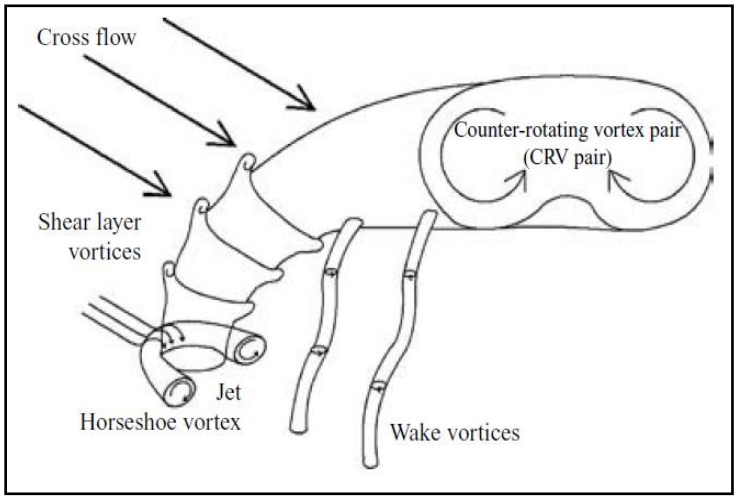

Figure 1.2: Regimes of the jet in cross-flow

Smith and Mungal (1998) also did an experimental study on JICF but with a circular jet. They investigated the effect of velocity ratio ranging from 5 to 25. Their study mainly concerns structural events in the vortex interaction region, mixing and mean centerline concentration decay. They revealed three regimes of jet and concluded that CRVP is asymmetric. This result is also given by Plesniak (2005) in study of confined squared JICF. Smith and Mungal observed that maximum centerline concentration decay along the centre-line coordinates occur at the rate of $s^{-1.3}$ in near field. Where 's' is the jet centerline coordinates. Then the rate slow down to $s^{-2/3}$ in the far field region.

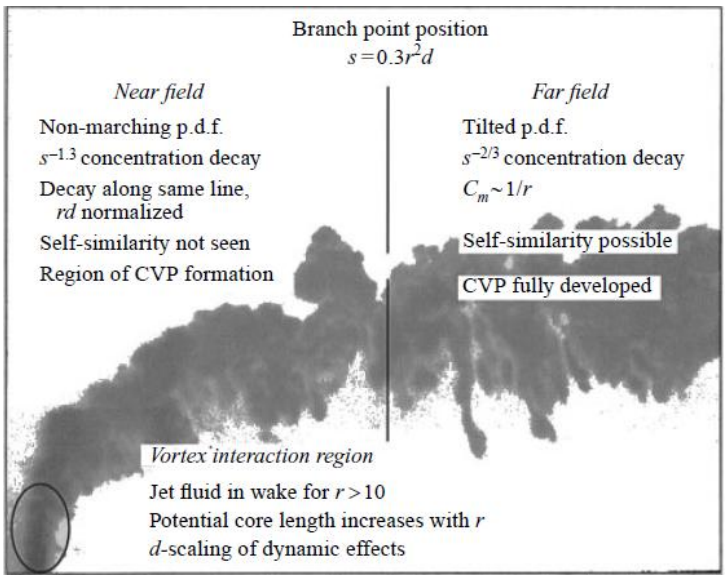

Figure 1.3: Features of the jet in cross-flow

Kevin Gosse (Gosse 2009) did experimental investigations on a small scale tunnel with obstacles built at TU Delft. A jet was injected through the floor to simulate accidental release of LPG in a road tunnel. He performed the experiment with three different jet flow-rates (Qj=255, 127.5 and 35 L/hr) with main stream velocity U_o=0.15 m/s. He measured mean value of concentration and standard deviation downstream the tunnel. It was concluded that scalar mixing is highly dependent upon jet flow-rate and presence of obstacles in the channel. For all jet flow-rates the concentration field is found to reach highest level in the central part between first pair of obstacles. Farther downstream, there were two different behaviors for different jet flow-rates. For the flow-rate QJ=255 L/h, the scalar field becomes homogeneous and symmetrical with respect of the mid-plane. For the flow-rate QJ=35 L/h, the scalar field is localized close to the ground floor and on the injection side of the channel, outside the wake zone of the obstacles. This experimental study was continued by J. Verdoold, who measured velocity field and turbulent kinetic energy with different jet velocity ($v_{jet} = 2.3\ m/s\ and\ 1.15\ m/s$). In this study, the results of J. Verdoold's experimental investigation have been used for validation of the models.

Inge Trijssenaar (2009) did numerical simulation of a road tunnel with obstacles. She used CFX and Ventunnel codes to simulate different cases. RNG k-ε turbulent model was used for modeling in CFX. Fluidyn Ventunnel is a CFD code dedicated to CFD modeling for road and rail tunnels. k-ε model was used for modeling in the Ventunnel codes. The concentration profile obtained from CFD simulation and experimental results were compared. Inge Trijssenaar simulated four different scenarios. Low and high jet velocity cases in experimental scale (water and salt water in lab scale) and in full scale (air and LPG in real tunnel) were modeled. Only the full scale case with low and high jet velocity was simulated using Ventunnel codes because it was not possible to use water as fluid in the Ventunnel code. It was concluded from the comparison of experimental and simulation results that for low jet velocity qualitative agreements is observed between the shapes of concentration profile. Ventunnel results were slightly better than CFX results. But quantitative agreement of computations and measurements was rather poor.

Ramezanizadeh, Taeibi-Rahni and Saidi (2007) did numerical simulation of a square cold jet in hot cross-flow. They studied the effect of density ratio on hydrodynamics of the jet. JICF was simulated using a large eddy simulation approach. They observed that CRVP was formed when the jet enters the cross-flow and two HSV formed at the lower corner beneath CRVP. They concluded that the density ratio has significant effect on the hydrodynamics of the jet. They found that by increasing the density ratio the diffusion of the CRVP increases and the jet penetrates and expands more into the cross-flow.

In the study of Wegner (2004) modeling of jet in cross-flow was performed using the large eddy simulation (LES) approach. The simulation was performed with different jet to cross-flow angles in order to enhance the mixing. It was observed that the jet angle has major effect on the mixing process. In our study the jet is injected into the cross-flow in vertical direction at the angle of 90^{o}. According to the study of Wegner (2004) we can state that our simulation can only be validated through the experiments in which jet and cross-flow are at right angle.

1.3. Experimental Setup

The experimental investigation is carried out on a small scale tunnel which is built at TU Delft. This small scale tunnel is a closed circuit rectangular channel, which is made of glass to take measurement efficiently. No probe or measuring device is inserted inside the channel which can affect the flow field. There are 27 obstacles mounted on the floor in two lines with 8 pairs of obstacles downstream the jet and 5 pairs of obstacles upstream. These obstacles are representing vehicles to simulate a traffic jam. At one obstacle position, there is an empty space and a square injection nozzle is placed there. The Jet is injected in vertical direction through this injection nozzle. The dimensions of tunnel and obstacles are given in Table 1.1 and these are shown in Figure 1.4 and Figure 1.5. In the experimental setup water is used as main stream representing air and saline solution (Sodium Chloride + Potassium Chloride + water), with higher density than water, is used as jet stream representing LPG. The reason of selecting water as main stream is to have high Reynolds number even with low main stream velocity. With main stream velocity equal to 0.15m/s Reynolds number is equal to 3.2×10^4 which is in the turbulence regime.

In the experimental investigation of the laboratory scale tunnel different cases have been studied. These are with different jet flow-rates and jet injection opening size. Essentially scalar concentration is measured and a report on the scalar concentrations is available (Gosse 2009). The concentration measurement technique is based on LIF technique, used by Brungart et al (1991), and a light-scattering technique. Recently, velocity measurements have been taken using the PIV technique by J. Verdoold. Besides velocity components, turbulent kinetic energy and uv Reynolds stress is also measured and recorded.

1.3.1. Scaling

The dimensions of a laboratory scale tunnel are scaled down from a real tunnel with 1:31.25 scaling ratio. In the design and scaling of experimental setup, Reynolds and Richardson dimensionless numbers are taken into account. Since water and saline solution are used to represent air and LPG respectively, it is important to have an equal strength of buoyancy force. This is characterized by Richardson number, which is ratio of potential to kinetic energy and given as:

$$Ri = \frac{g\Delta\rho h}{\rho U_\infty^2}$$

In the real tunnel case with ventilation air velocity, U_∞ = 3 m/s, and density ratio of air to LPG, $\Delta\rho/\rho$ = 0.7755, the Richardson number is *Ri* = 1.3. In the experimental case, where air is replace with water and LPG with saline solution, in order to get identical *Ri* number, density ratio should be equal to 0.06. This is achieved by having density of saline solution equal to 1060 kg/m^3.

From literature review, it appears that another important parameter to characterize JICF is scaled velocity ratio, *r*, given as:

$$r = \left(\frac{\rho_j}{\rho_f}\right)^{0.5} \frac{U_j}{U_f}$$

Where, ρ_j and ρ_f are densities of jet and main stream and U_j and U_f are velocities of jet and main stream respectively. This ratio can also be described as the square root of the momentum flux ratio. The scaled velocity ratio in the case of a real tunnel with air and LPG is equal to 15.8. In order to have identical value of velocity ratio at laboratory scale with water and saline solution the jet velocity should be around 3m/s. This is why the experiment is performed with jet velocity of 2.3 m/s. The jet with 2.3 m/s velocity is injected through 5x5mm nozzle opening.

From the kinematic viscosity of the saline solution, $\nu_j = 9.81 \times 10^{-7}$, determined by Hai-Lang and Shi-Jun (1996) with density 1060 kg/m3 and temperature 298K, the Reynolds number based on the nozzle dimension can be calculated and it is equal to 1.2×10^4 for the jet, which is also in the turbulent region. According to scaling rules presented by Roekaerts if the scaling is done at constant I_{ratio} given as

$$I_{ratio} = \frac{\rho_{jet}\, U_{jet}^2}{\rho_{flow}\, U_{flow}^2}$$

the mixing features of the jet will be preserved. In this study scaling is done with constant I_{ratio} so that the mixing features of jet will be preserved. Also if the scaling is done at constant Vol_{ratio} , the location of the volume based stoichiometric contour is preserved. The Vol_{ratio} is given as

$$Vol_{ratio} = \frac{U_{jet}\, A_{jet}}{U_{flow}\, A_{flow}}$$

In our case, the volume ratio is not constant. In case of real tunnel $Vol_{ratio} = 0.0075$ and in the experimental case $Vol_{ratio} = 0.0057$.

Table 1.1: Dimensions of experimental and full scale tunnel

	Experimental Scale (m)	**Full Scale (m)**
Tunnel		
Tunnel Height	0.16	5
Tunnel width	0.32	10
Tunnel length	4	125
Obstacles or Cars		
Height	0.049	1.5
Width	0.056	1.8
Length	0.136	4.3
Distance between obstacles	0.064	2
Jet source dimension (Length x Width)	0.005 x 0.005	0.156x0.156

Table 1.2: Parameters

	Experimental Scale	**Full Scale**
Cross-flow stream		
Fluid	Water	Air
Velocity (m/s)	0.15	3
Density (kg/m3)	1000	1.205
Reynolds number *Re*	$3.2x10^4$	$1.2x10^6$
Richardson number *Ri*	1.3	1.3
Jet Stream		
Fluid	Saline solution	LPG
Density (kg/s)	1060	2.175
Velocity (m/s)	2.3	35.3
Reynolds number *Re*	$1.2x10^4$	$6.0x10^5$

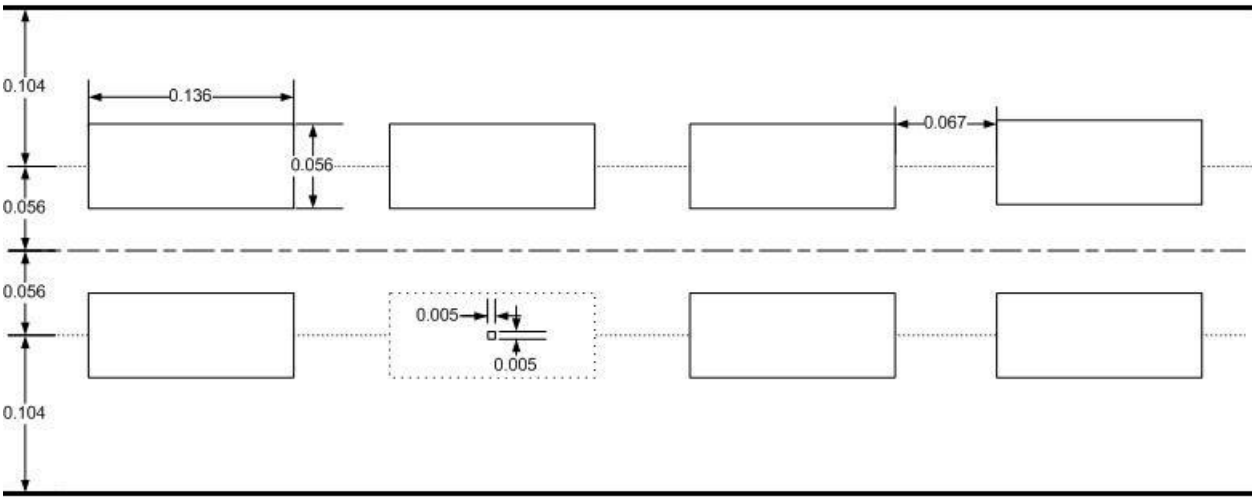

Figure 1.4: Tunnel top view

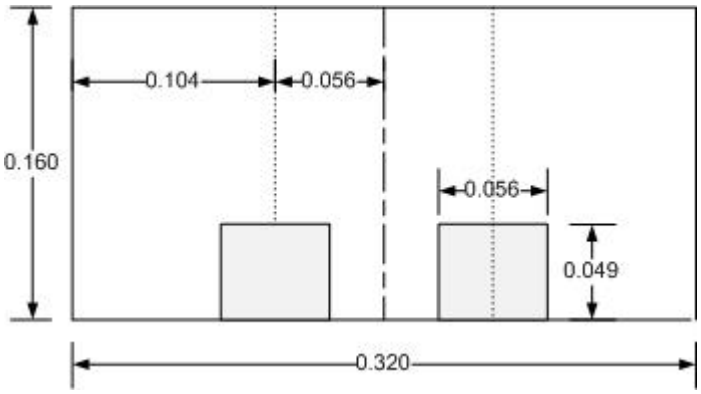

Figure 1.5: Tunnel front view

CHAPTER 2

THEORY

In this chapter, the governing equations and the turbulence models used for simulation are explained. When using FLUENT for simulation, Reynolds Stress Model has been employed for turbulence modeling and for near wall modeling, 'enhanced wall treatment' approach has been used. On the other hand, when using In-house codes for simulation, standard k-ε and modified k-ε models have been tested and for near wall modeling, 'wall function' has been used.

2.1. Governing Equations

Basic governing equations solved are mass continuity equation and momentum transport equation. For incompressible flow mass continuity equations is given as:

$$\frac{\partial \widetilde{U_j}}{\partial x_j} = 0$$

And momentum transport equation is given as:

$$\frac{\partial(\rho \widetilde{U_i})}{\partial t} + \widetilde{U_j}\frac{\partial(\rho \widetilde{U_i})}{\partial x_j} = -\frac{\partial \tilde{P}}{\partial x_i} - \frac{\partial \tau_{ji}}{\partial x_j} + \rho g_i$$

Where $\tilde{P}$ is the static pressure, g_i is acceleration due to gravity and τ_{ji} is stress tensor. For incompressible Newtonian fluids, the stress tensor, τ_{ji}, is given as:

$$\tau_{ji} = -\rho\nu\left(\frac{\partial \widetilde{U_i}}{\partial x_j} + \frac{\partial \widetilde{U_j}}{\partial x_i}\right)$$

Here ν is kinematic viscosity. Then momentum transport equation becomes:

$$\frac{\partial(\rho \widetilde{U_i})}{\partial t} + \widetilde{U_j}\frac{\partial(\rho \widetilde{U_i})}{\partial x_j} = -\frac{\partial \tilde{P}}{\partial x_i} - \nu\frac{\partial^2(\rho \widetilde{U_i})}{\partial x_j \partial x_j} + \rho g_i$$

These equations are collectively referred to as Navier-Stokes equations. These equations are directly solved in ''direct numerical simulation'' (DNS). Very fine mesh is required to solve these equations. This is computationally very expensive and solving industrial application using DNS is not practicable.

In the Navier-Stokes equations velocity, $\widetilde{U_i}$, and pressure, $\tilde{P}$, are instantaneous values. Instantaneous values are very difficult to find. According to Reynolds' proposal these instantaneous values can be decomposed into average and fluctuation part.

$$\widetilde{U_i} = U_i + u_i$$

$$\tilde{P} = P + p$$

Where U_i and P are mean component and u_i and p are fluctuation part. The decomposition of instantaneous values into mean and fluctuation part is called Reynolds decomposition. By definition the average of fluctuations is zero.

$$\langle u_i \rangle = 0$$

$$\langle p \rangle = 0$$

Here brackets, ⟨ ⟩, indicates averaging over time. When Reynolds decomposition is applied on Navier-Stokes equations and these are averaged over a time period we obtain a set of equations given as:

$$\frac{\partial U_i}{\partial x_i} = 0$$

$$\frac{\partial U_i}{\partial t} + U_j \frac{\partial U_i}{\partial x_j} = -\frac{1}{\rho}\frac{\partial}{\partial x_j}\left\{P\delta_{ij} + \left(\frac{\partial U_i}{\partial x_j} + \frac{\partial U_j}{\partial x_i}\right) - \rho\langle u_i u_j\rangle\right\} + g_i$$

This equation is known as Reynolds averaged Navier-Stokes (RANS) equation. In this equation $\rho\langle u_i u_j\rangle$ is referred to as Reynolds stresses and it is very important since it introduces coupling between mean and fluctuating parts of velocity. Its value cannot be calculated from the mean value. So it should be modeled in order to close the equation. In the following section the modeling of Reynolds stress term is discussed.

2.2. Turbulence Models

Turbulence models are used to model the Reynolds stress tensor. There are different approaches to model this term.

2.2.1. Turbulence models based on Bousinessq Hypothesis

According to Bousinessq Hypothesis Reynolds stress tensor can be modeled using turbulent viscosity and it is proportional to strain rate tensor

$$\langle u_i u_j\rangle = \frac{2}{3}k\delta_{ij} - 2\nu_t S_{ij}$$

Where δ_{ij} is Kronecker delta function and ν_t is turbulent viscosity. Strain rate tensor, S_{ij}, is given as

$$S_{ij} = \frac{1}{2}\left(\frac{\partial U_i}{\partial x_j} + \frac{\partial U_j}{\partial x_i}\right)$$

There are different approached to find the value of turbulent viscosity. According to these approaches turbulent viscosity can be calculated using appropriate length and time scale.

2.2.1.1. Standard *k-ε* model

In Standard *k-ε* turbulence model two transport equations are solved (transport equation for turbulent kinetic energy, *k*, and dissipation rate, ε) in order to calculate turbulent viscosity. Using these quantities turbulent viscosity is calculated as:

$$\nu_t = C_\mu \frac{k^2}{\varepsilon}$$

Where $C_\mu = 0.09$. In standard *k-ε* model the transport equation for turbulent kinetic energy, *k*, is given as

$$\frac{\partial k}{\partial t} + U_j \frac{\partial k}{\partial x_j} = \frac{\partial}{\partial x_j}\left[\left(\nu + \frac{\nu_t}{\sigma_k}\right)\frac{\partial k}{\partial x_j}\right] + P_k - \varepsilon$$

Where $\sigma_k = 0.7$ and P_k is the production of *k*. This term is modeled using rate of strain tensor as

$$P_k = -\langle u_i u_j \rangle \frac{\partial U_i}{\partial x_j} = \nu_t \left(\frac{\partial U_i}{\partial x_j} + \frac{\partial U_j}{\partial x_i}\right)\frac{\partial U_i}{\partial x_j} = 2\nu_t S_{ij} S_{ij} = \nu_t |S|^2$$

The transport equation for dissipation rate, ε, is given as

$$\frac{\partial \varepsilon}{\partial t} + U_j \frac{\partial \varepsilon}{\partial x_j} = \frac{\partial}{\partial x_j}\left[\left(\nu + \frac{\nu_t}{\sigma_\varepsilon}\right)\frac{\partial \varepsilon}{\partial x_j}\right] + C_{\varepsilon 1}\frac{\varepsilon}{k}P_k - C_{\varepsilon 2}\rho\frac{\varepsilon^2}{k}$$

Where $C_{\varepsilon 1} = 1.42$, $C_{\varepsilon 2} = 1.68$ and $\sigma_\epsilon = 0.7$.

2.2.1.2. Modified *k-ε* model: Durbin time scale limiter modification

Standard *k-ε* model over predicts the value of turbulent kinetic energy, *k*, in the stagnant region. There are several studies available which show that Durbin time scale limiter improves results when there are stagnant areas in the flow. In this domain there are low velocity region behind obstacles. This is why Durbin time scale limiter is applied in this study. Durbin time scale limiter is correction for the over prediction of *k* near stagnation points in flows by applying a limiter on the turbulent time scale k/ε as

$$T = min\left[\frac{k}{\varepsilon}, \frac{0.6}{\sqrt{6}C_\mu |S|}\right]$$

This limiter is applied on the production term in the transport equation of ε. This results in a higher production of ε and thus a reduction of *k*. The Durbin time scale limiter is also applied in the equation of turbulent viscosity, ν_t. When the limiter is applied the equation for turbulent viscosity, ν_t, and the dissipation rate, ε, are given as

$$\nu_t = C_\mu kT$$

$$\frac{\partial \varepsilon}{\partial t} + U_j \frac{\partial \varepsilon}{\partial x_j} = \frac{\partial}{\partial x_j}\left[\left(\nu + \frac{\nu_t}{\sigma_\varepsilon}\right)\frac{\partial \varepsilon}{\partial x_j}\right] + \frac{C_{\varepsilon 1} P_k - C_{\varepsilon 2}\varepsilon}{T}$$

2.2.2. Reynolds Stress Model

Another approach to find the value of Reynolds stress tensor is by directly solving transport equation of Reynolds stresses. The cost of this is now seven extra transport equations should be solved. Six for Reynolds stresses and one for turbulent dissipation rate, ε. These equations are susceptible to numerical instability since they are strongly coupled. However it gives better results when Reynolds stresses are anisotropic and Boussinesq approximation is not valid. The transport equation of Reynolds stress solved by FLUENT is given as:

$$\underbrace{\frac{\partial}{\partial t}\left(\rho\langle u_i u_j\rangle\right)}_{\text{Local Time Derivative}} + \underbrace{\frac{\partial}{\partial x_k}\left(\rho U_k \langle u_i u_j\rangle\right)}_{C_{ij}\,=\,Convection} = -\underbrace{\frac{\partial}{\partial x_k}\left[\rho\langle u_i u_j u_k\rangle + \langle p\left(\delta_{kj}u_i + \delta_{ik}u_j\right)\rangle\right]}_{D_{T,ij}\,=\,Turbulent\ Diffusion}$$

$$\underbrace{+\frac{\partial}{\partial x_k}\left[\mu\frac{\partial}{\partial x_k}\langle u_i u_j\rangle\right]}_{D_{L,ij}\,=\,Molecular\ Diffusion} \underbrace{-\rho\left(\langle u_i u_k\rangle\frac{\partial U_j}{\partial x_k} + \langle u_j u_k\rangle\frac{\partial U_i}{\partial x_k}\right)}_{P_{ij}\,=\,Stress\ Production} \underbrace{-\rho\beta\left(g_i\langle u_j\theta\rangle + g_i\langle u_i\theta\rangle\right)}_{G_{ij}\,=\,Buoyancy\ Production}$$

$$\underbrace{+\langle p\left(\frac{\partial u_i}{\partial x_j} + \frac{\partial u_j}{\partial x_i}\right)\rangle}_{\phi_{ij}\,=\,Pressure\ Strain} \qquad \underbrace{-2\mu\langle\frac{\partial u_i}{\partial x_k}\frac{\partial u_j}{\partial x_k}\rangle}_{\varepsilon_{ij}\,=\,Dissipation}$$

$$\underbrace{-2\rho\Omega_k\left(\langle u_j u_m\rangle\varepsilon_{ikm} + \langle u_i u_m\rangle\varepsilon_{jkm}\right)}_{F_{ij}\,=\,Production\ by\ System\ Rotation}$$

In this equation the terms C_{ij}, $D_{L,ij}$, P_{ij} and F_{ij} do not require any modeling. Whereas the terms $D_{T,ij}$, G_{ij}, ϕ_{ij} and ε_{ij} need to be modeled to close the equation. In the following section modeling of these terms is discussed individually.

2.2.2.1. Modeling Turbulent Diffusive Transport

$D_{T,ij}$ is modeled by the generalized gradient diffusion model. The simplified equation is given as:

$$D_{T,ij} = \frac{\partial}{\partial x_k}\left(\frac{\mu_t}{\sigma_k}\frac{\partial\langle u_i u_j\rangle}{\partial x_k}\right)$$

Where μ_t is turbulent viscosity and it is computed using equation:

$$\mu_t = \rho C_\mu \frac{k^2}{\epsilon}$$

Where $C_\mu = 0.09$ and $\sigma_k = 0.82$

2.2.2.2. Modeling the pressure strain term

Many different models are suggested to model pressure strain term each having validity for specific case. The model used in this simulation is Linear Pressure Strain Model including wall reflection term proposed by Gibson and Launder (1978).

2.2.2.2.1. Linear Pressure Strain Model

In Linear Pressure Strain Model, pressure strain term is decomposed into parts as follows

$$\phi_{ij} = \phi_{ij,1} + \phi_{ij,2} + \phi_{ij,w}$$

Where $\phi_{ij,1}$ is slow pressure strain term. This term tries to make stresses isotropic. $\phi_{ij,2}$ is rapid pressure strain term and $\phi_{ij,w}$ is the wall reflection term. The slow pressure strain term, $\phi_{ij,1}$, is modeled as:

$$\phi_{ij,1} = -C_1 \rho \frac{\varepsilon}{k}\left[\langle u_i u_j \rangle - \frac{2}{3}\delta_{ij} k\right]$$

Where $C_1 = 1.8$

The rapid pressure strain term, $\phi_{ij,2}$, is modeled as:

$$\phi_{ij,2} = -C_2\left[\left(P_{ij} + F_{ij} + G_{ij} - C_{ij}\right) - \frac{2}{3}\delta_{ij}\left(P + G - C\right)\right]$$

Where $C_2 = 0.6$.

P_{ij}, F_{ij}, G_{ij}, and C_{ij} are already defined in transport equation of Reynolds stresses. $P = 0.5P_{kk}$, $G = 0.5G_{kk}$ and $C = 0.5C_{kk}$.

The wall reflection term, $\phi_{ij,w}$, tries to redistribute normal stresses near the wall. It tends to damp the normal stress perpendicular to the wall while enhancing the stresses parallel to wall. This term is modeled as:

$$\phi_{ij,w} = C_1^{'}\frac{\varepsilon}{k}\left(\langle u_k u_m \rangle n_k n_m \delta_{ij} - \frac{3}{2}\langle u_i u_k \rangle n_j n_k - \frac{3}{2}\langle u_j u_k \rangle n_i n_k\right)\frac{C_l k^{3/2}}{\varepsilon d}$$

$$+C_2^{'}\left(\phi_{km,2} n_k n_m \delta_{ij} - \frac{3}{2}\phi_{ik,2} n_j n_k - \frac{3}{2}\phi_{jk,2} n_i n_k\right)\frac{C_l k^{3/2}}{\varepsilon d}$$

Where $C_1^{'} = 0.5$, $C_2^{'} = 0.3$, and n_k is the x_k component of the unit normal to the wall, d is the normal distance from the wall.

$$C_l = C_\mu^{3/4}/\kappa$$

Where $C_\mu = 0.09$ and κ is the von Karman constant ($\kappa = 0.4187$)

2.2.2.2.2. Low-Re Modifications to linear pressure strain model

When the RSM is applied to near wall flows using the ''enhanced wall treatment'', which is used in this simulation, the pressure strain model is modified. In the modification the values of C1, C2, C1' and C2' are specified as function of Reynolds stress invariants and turbulent Reynolds number and these constants are now given as

$$C_1 = 1 + 2.58A\sqrt{A_2}\{1 - exp[-(0.0067Re_t)^2]\}$$

$$C_2 = 0.75\sqrt{A}$$

$$C_1^{'} = -\frac{2}{3}C_1 + 1.67$$

$$C_2^{'} = max\left[\frac{\frac{2}{3}C_2 - \frac{1}{6}}{C_2}, 0\right]$$

Where turbulent Reynolds number, Re_t, is given as

$$Re_t = (\rho k^2/\mu\epsilon)$$

The parameter A and tensor invariants A2 and A3 are given by the following equations

$$A = \left[1 - \frac{9}{8}(A_2 - A_3)\right]$$

$$A_2 = a_{ik}\,a_{ki}$$

$$A_3 = a_{ik}\,a_{kj}\,a_{ji}$$

a_{ij} is the Reynolds stress anisotropy tensor given as:

$$a_{ij} = -\left(\frac{-\rho\langle u_i u_j\rangle + \frac{2}{3}\rho k\delta_{ij}}{\rho k}\right)$$

These low Re modifications only apply when enhanced wall treatment is used for near wall modeling. As in this simulation enhanced wall treatment is used for near wall modeling so these modifications are applied.

2.2.2.3. Effect of Buoyancy on turbulence

The production term due to buoyancy important when there is temperature gradient. Since temperature is same throughout the domain and energy is not solved in this simulation so the buoyancy term is not included.

2.2.2.4. Modeling the turbulence kinetic energy

Throughout the domain of flow, when the turbulence kinetic energy is required for modeling a specific term, it is obtained from the Reynolds stress tensor as:

$$k = \frac{1}{2}\langle u_i u_i \rangle$$

However, to obtain values of Reynolds stresses for boundary conditions FLUENT solves a transport equation of turbulent kinetic energy. It is identical to transport equation used in the standard *k-ε* model. This is given as:

$$\frac{\partial}{\partial t}(\rho k) + \frac{\partial}{\partial x_i}(\rho k u_i) = \frac{\partial}{\partial x_j}\left[\left(\mu + \frac{\mu_t}{\sigma_k}\right)\frac{\partial k}{\partial x_j}\right] + \frac{1}{2}(P_{ii} + G_{ii}) - \rho\epsilon(1 + 2M_t^2)$$

Where $\sigma_k = 0.82$.

Although this equation is solved throughout the flow domain, the values of k obtained are used only for boundary conditions. In every other case, *k* is obtained from Reynolds stress tensor.

2.2.2.5. Modeling the Dissipation rate

The dissipation tensor is modeled as an isotropic tensor for compressible flow. Since in this simulation flow is assumed to be incompressible this modification is neglected. The scalar dissipation rate ε is computed from a transport equation similar to that used in the standard *k-ε* model:

$$\frac{\partial}{\partial t}(\rho\varepsilon) + \frac{\partial}{\partial x_i}(\rho\varepsilon u_i) = \frac{\partial}{\partial x_j}\left[\left(\mu + \frac{\mu_t}{\sigma_k}\right)\frac{\partial \varepsilon}{\partial x_j}\right] C_{\varepsilon 1}\frac{1}{2}[P_{ii}]\frac{\epsilon}{k} - C_{\varepsilon 2}\rho\frac{\varepsilon^2}{k}$$

Where $\sigma_k = 1.0$, $C_{\varepsilon 1} = 1.44$, $C_{\varepsilon 2} = 1.92$.

2.3. Modeling of Specie transport

Conservation equation for specie is given as

$$\frac{\partial \rho \widetilde{Y}_i}{\partial t} + U_j\frac{\partial \rho \widetilde{Y}_i}{\partial x_j} = \frac{\partial}{\partial x_j}\left[\frac{\mu}{Sc}\left(\frac{\partial \widetilde{Y}_i}{\partial x_j}\right)\right]$$

Where *Sc* is Schmidt number and given as

$$Sc = \frac{\mu}{\rho D_{AB}} = 609$$

Analogous to instantaneous velocity, in the conservation equation for momentum, $\widetilde{Y}_i$ is the instantaneous mass fraction of ith specie. The Reynolds decomposition for instantaneous mass fraction is

$$\widetilde{Y}_i = Y_i + y_i$$

Where instantaneous mass fraction, $\widetilde{Y}_i$, is decomposed to average mass fraction Y_i and fluctuating part y_i. After applying Reynolds decomposition and Reynolds averaging to this equation we get

$$\frac{\partial Y_i}{\partial t} + U_j \frac{\partial Y_i}{\partial x_j} = \frac{\partial}{\partial x_j}\left[\frac{\nu}{Sc}\left(\frac{\partial Y_i}{\partial x_j}\right) - \langle y_i u_j \rangle\right]$$

In this equation turbulent concentration fluxes, $\langle y_i u_j \rangle$, is unknown and it needs to be modeled. It represents the transport of concentration due to fluctuating velocity. In this study it is modeled by ''simple gradient diffusion hypothesis''.

2.3.1. Simple Gradient Diffusion Hypothesis

In Simple Gradient Diffusion Hypothesis it is assumed that the turbulent concentration flux, $\langle y_i u_j \rangle$, is proportional to the gradient of mean concentration.

$$-\langle y_i u_j \rangle = \mathcal{D}_t \frac{\partial Y_i}{\partial x_j}$$

Where proportionality constant $\mathcal{D}_t = \nu_t / Sc_t$ is the eddy diffusivity and Sc_t is the turbulent Schmidt number. Its value is 0.7 in this study.

2.4. Near wall modeling

Wall functions are used to model the near wall region. In the near wall region viscous effects are dominating and turbulence models are not applicable in this region. In this region rapid variation of flow variables occurs. This means that a very fine mesh is required to accurately resolve the steep gradients of flow variables, which can make CFD simulation computationally expensive. There are two approaches used to model near wall region. First is that the viscosity affected near wall region is not resolved and wall functions are used to obtain boundary conditions for the mean velocity components and the turbulent quantities at the first grid point far from wall.

In this study when *k-ε* turbulent model is selected, near wall modeling is performed by ''wall functions''. On the other hand when Reynolds stress model is selected ''enhanced wall treatment'' approach is used. In this selection both the wall function and enhanced wall treatment approach have been discussed individually.

2.4.1. Wall function

As explained earlier, the turbulent models require values of parameter at first grid point close to the wall. This is provided by wall functions. At high Reynolds number the dimensionless velocity is independent of viscosity and behaves as

$$U^+ = \frac{1}{\kappa}\ln(Ey^+)$$

Where $\kappa = 0.41$ is the von Karman constant, $E = 8.432$ is the log-law constant for a smooth wall and the dimensionless wall velocity is U^+ defined as

$$U^+ = \frac{U}{u_\tau}$$

Where u_τ is the friction velocity given as

$$u_\tau = \sqrt{\frac{\tau_w}{\rho}}$$

And τ_w is the wall shear stress. The dimensionless wall distance is given as

$$y^+ = \frac{u_\tau y}{\nu}$$

2.4.2. Enhanced wall treatment

Enhanced wall treatment is a near-wall modeling method that is a combination of a two-layer model and enhanced wall functions. The two layer model requires very fine mesh (typically y+ = 1). However this requirement can make simulation computationally very expensive. On the other hand wall function does not require very fine mesh. This increases validity of enhanced wall treatment from very fine mesh to relatively coarse mesh. The enhanced wall treatment uses a blending function to smoothly transfer from wall function and two-layer model to turbulence model in the main flow.

The enhanced wall treatment approach possesses the accuracy of the standard two-layer approach for fine near-wall meshes and at the same time does not reduce accuracy for wall-function meshes. Since the current case consists of complex geometry which involves flow separation, ordinary wall functions could not give sufficient accuracy. This is why enhanced wall treatment approach is applied in this simulation. Typical mesh requirement when using enhanced wall treatment is that y+ value should be y+ < 5. However, enhanced wall treatment is valid for coarse mesh as well. The current mesh has y+ values near wall from 2.5 < y+ < 25.

2.4.2.1. Two-Layer Model for Enhanced Wall Treatment

The two-layer approach is an integral part of the enhanced wall treatment and it specifies both dissipation rate, ε, and the turbulent viscosity, μ_t, in the near-wall cells. In this approach, the whole domain is subdivided into two layers, a viscosity-affected region and a fully-turbulent region. These two regions are identified by a wall-distance-based, turbulent Reynolds number, Re_y, defined as

$$Re_y = \frac{\rho y \sqrt{k}}{\mu}$$

$$\begin{aligned} &Fully\ turbulent\ region\ when && Re_y > Re_y^*;\ Re_y^* = 200 \\ &Viscosity\ affected\ region\ when && Re_y < Re_y^*;\ Re_y^* = 200 \end{aligned}$$

Where, *y* is the normal distance from the wall to the cell centers. In FLUENT, *y* is interpreted as the distance to the nearest wall.

In the fully turbulent region, the Reynolds Stress Model is employed. In the viscosity-affected near-wall region, the one-equation model of Wolf-stein (1969) is employed. In this one-equation model, the momentum equations and the transport equation of turbulent kinetic energy, *k*, are solved. However, the turbulent viscosity, μ_t, is now computed from

$$\mu_{t,2layer} = \rho C_\mu l_\mu \sqrt{k}$$

And

$$l_\mu = y C_l^* \left(1 - e^{-Re_y / A_\mu}\right)$$

In the two layer model, viscosity, $\mu_{t,2layer}$, is smoothly blended with high Reynolds number viscosity, μ_t, using a blending function as

$$\mu_{t,enh} = \lambda_\varepsilon \mu_t + (1 - \lambda_\epsilon)\mu_{t,2layer}$$

A blending function, λ_ε , is defined as it is equal to unity far from walls and is zero very near to walls.

The turbulent dissipation rate, ε, is computed from

$$\varepsilon = \frac{k^{3/2}}{l_\varepsilon}$$

And

$$l_\varepsilon = y C_l^* \left(1 - e^{-Re_y / A_\varepsilon}\right)$$

The constants are given as

$$C_l^* = \kappa C_\mu^{-3/4}, A_\mu = 70, A_\varepsilon = 2C_l^*$$

2.4.2.2. Enhanced Wall Functions

Enhanced wall function extends the applicability of enhanced wall treatment approach throughout the near wall region (i.e., laminar sub-layer, buffer region, and fully-turbulent outer region). In enhanced wall function linear (laminar) and logarithmic (turbulent) laws of wall are blended smoothly using a blending function as

$$u^+ = e^{\Gamma} u_{lam}^+ + e^{\frac{1}{\Gamma}} u_{turb}^+$$

And blending function Γ is

$$\Gamma = -\frac{a(y^+)^4}{1 + by^+}$$

Where a = 0.01 and b = 5.

Similarly the equation for the derivative is given as

$$\frac{du^+}{dy^+} = e^{\Gamma} \frac{du_{lam}^+}{dy^+} + e^{\frac{1}{\Gamma}} \frac{du_{turb}^+}{dy^+}$$

The enhanced turbulent law of wall for compressible flow with heat transfer and pressure gradients has been derived by combining the approaches of White and Cristoph (1971) and Huang et al. (1993) and it is given as

$$\frac{du_{turb}^+}{dy^+} = \frac{1}{\kappa y^+} [S^{'}(1 - \beta u^+ - \gamma (u^+)^2)]^{1/2}$$

Where

$$S^{'} = \begin{Bmatrix} 1 + \alpha y^+ \; for \; y^+ < y_s^+ \\ 1 + \alpha y_s^+ \; for \; y^+ \geq y_s^+ \end{Bmatrix}$$

And

$$\alpha = \frac{v_w}{\tau_w u^*} \frac{dp}{dx} = \frac{\mu}{\rho^2 (u^*)^3} \frac{dp}{dx}$$

$$\beta = \frac{\sigma_t q_w u^*}{c_p \tau_w T_w} = \frac{\sigma_t q_w}{\rho c_p u^* T_w}$$

$$\gamma = \frac{\sigma_t (u^*)^2}{2 c_p T_w}$$

The default value is, $y_s^+ = 60$. The coefficient α in the equation represents the influences of pressure gradients while the coefficients β and γ represent thermal effects.

The laminar law of wall is determined from the following equation

$$\frac{du_{lam}^+}{dy^+} = 1 + \alpha y^+$$

In this expression only the effect of pressure gradients through α are included. While the effect of heat transfer and compressibility on the 'laminar wall law' are neglected, because these effects have minor importance in the region close to the wall.

CHAPTER 3

FLUENT: Simulation Setup

The geometry, mesh and boundary conditions employed for simulation using FLUENT are presented in this chapter. The discretization scheme used for simulation is first order upwind scheme. Although it is true that first order upwind scheme is very diffusive but we could not get solution converged with higher order upwind scheme. We can decrease numerical diffusion by using structured mesh and by using fine mesh. This decreases the numerical diffusion. This is why in this simulation structured and fine mesh is used instead of using higher order discretization scheme.

3.1. Geometry

The geometry of the tunnel is created to exactly represent the experimental configuration. Details about the dimensions of tunnel and obstacles are given Table 1.1. For the case of the simulation, tunnel is made 4 m long with 27 obstacles. Figure 3.1 a) shows the geometry of tunnel created, using built-in geometry software of ANSYS work-bench. The figure shows that there is part of tunnel downstream without obstacles. This part is made to study dispersion of saline solution in far downstream region. The jet injection point is placed at 1.218 m in x direction from inlet and at z = 0.056 m. This is because the inlet conditions do not affect the area of interest i.e. the area near the jet injection. In the upstream region the flow becomes fully developed before it reaches the jet. Figure B1 in Appendix B shows velocity contours at different locations in the tunnel. It can be seen that the flow is fully developed before it has reached close to the jet. Similarly the tunnel outlet is far away from the jet so that the outflow also has no effect on the area of interest.

The jet is injected through a long straight square pipe. The flow is fully developed in the pipe before it enters the cross-flow stream. The simulation of the injection pipe is done separately. A 5x5mm pipe with 0.1 m length is created. And simulation is done to have a fully developed flow profile which enters into the main flow. Figure 3.1 b) shows the geometry of jet inlet pipe which is created using Gambit.

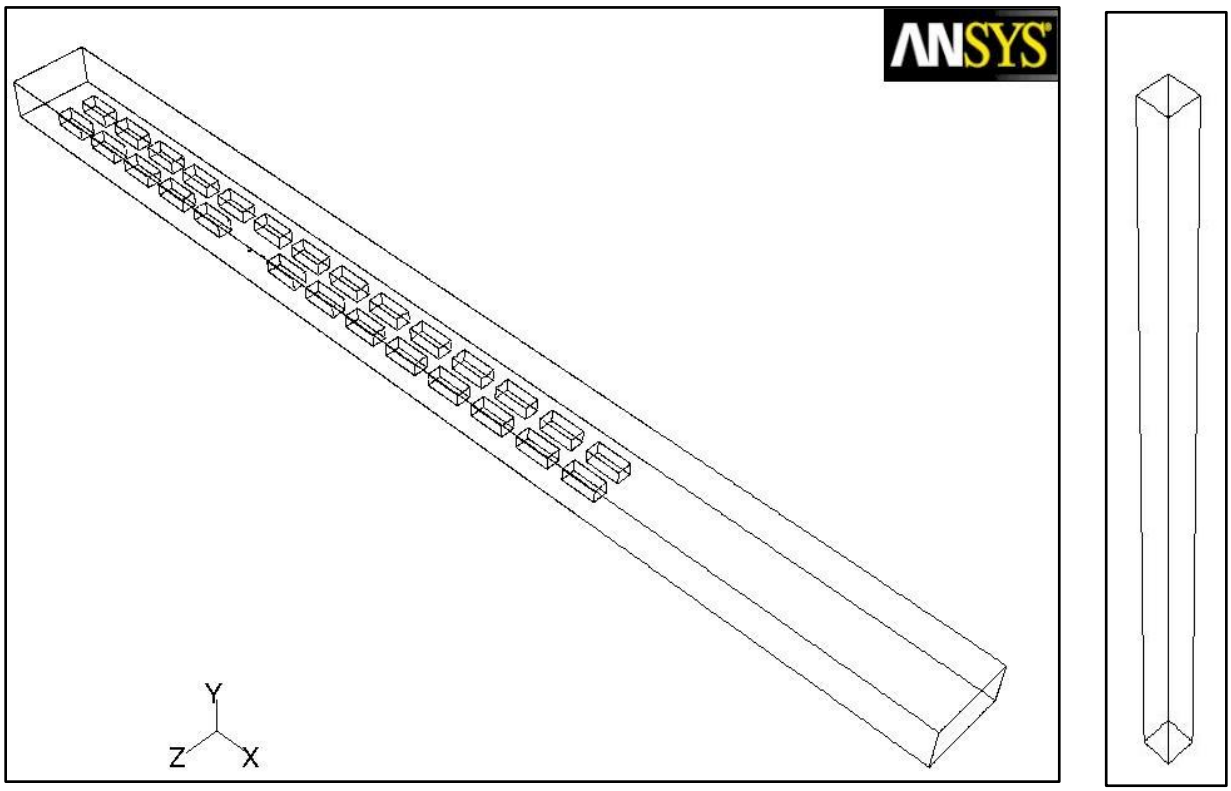

Figure 3.1: a) shows geometry of the tunnel and b) shows the geometry of the inlet pipe

3.2. Mesh

Meshing of the geometry is necessary to divide full computational domain into small volumes called cells. Here the built-in ANSYS work-bench meshing software and Gambit is used to mesh. The mesh is structured and composed of hexahedral cells. Hexahedral cells are preferred because then the solution converges quickly. It is also important to note mesh's maximum aspect ratio and cell skewness. The acceptable value of maximum cell skewness is less than 0.95 and average below 0.33. The aspect ratio should be below 5 but up to 10 inside the boundary layer is acceptable. The Meshes in which simulation is done fulfill these criteria. Mesh characteristics are presented in Table 3.1. Initially simulation is done on a course mesh with 0.8 Million cells. Then the mesh is refined several times to obtain grid independent solution. The solution is supposed to be grid independent when further refining the mesh does not influence the results. By refining the mesh finally a grid independent solution is obtained. The mesh have y+ value near wall from $2.5 < y+ < 25$.

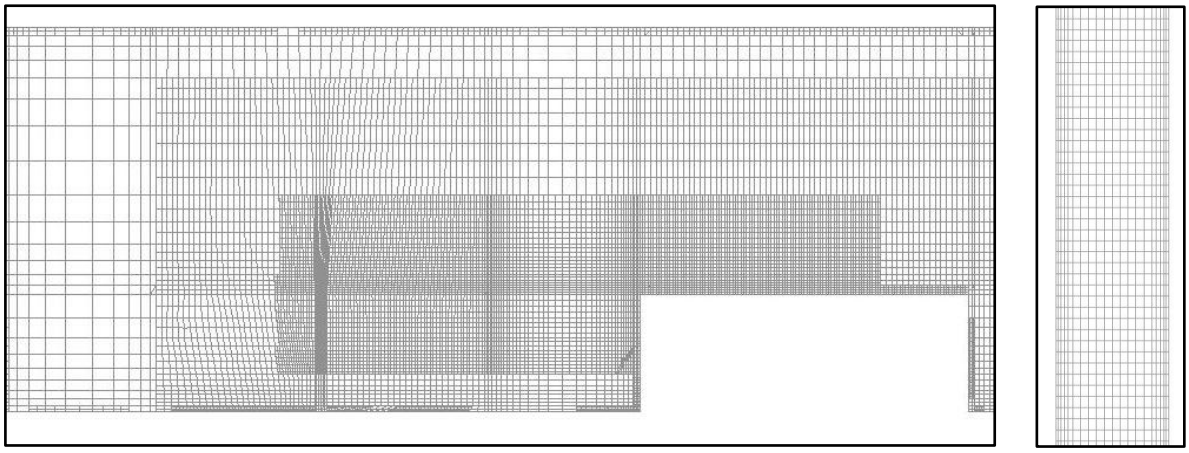

Figure 3.2: a) mesh of tunnel at the location of jet injection and b) mesh of LPG inlet

Table 3.1: Mesh characteristics

	Tunnel Mesh		**Jet inlet Mesh**
	Before refinement	**After Refinement**	
Number of Cells	802230	2381535	80000
Number of Nodes	867477	2871562	88641
Maximum aspect ratio	10	10	6.2
Maximum cell skewness	0.59	0.8568	0

After refining the mesh to 2.38 Million cells the solution finally obtained is grid independent. Figure 3.3 shows simulation results with different grids. This is U velocity plot along x direction at z = 0.104m and

y/h = 0.8. It is clear that results with grids having 2.14 M and 2.38 M cells are exactly coinciding. So the results with grid having 2.38 M cells are considered as grid independent.

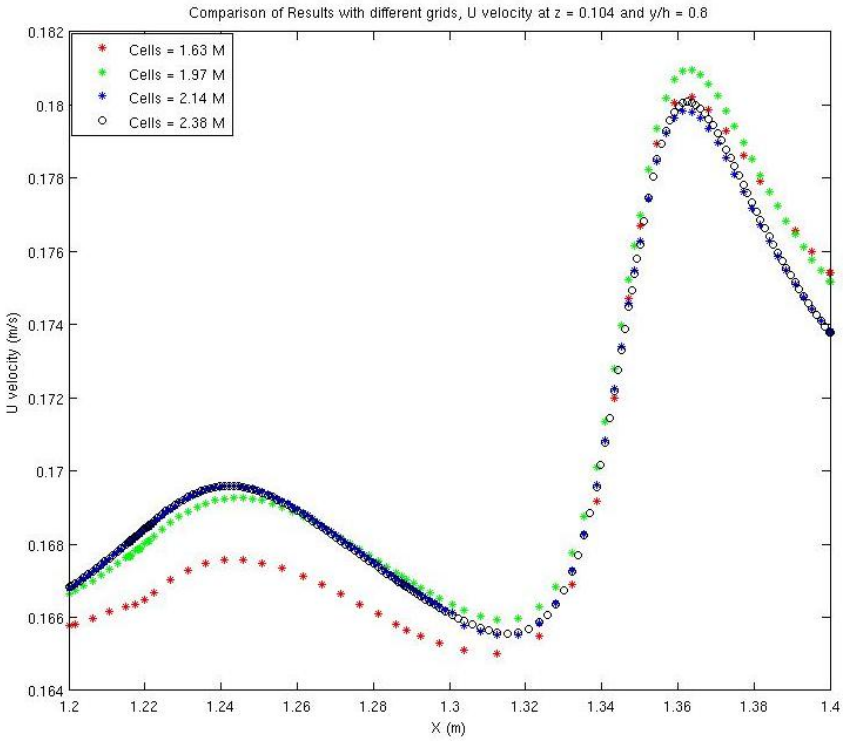

Figure 3.3: Comparison of results with different grids

3.3. Specifying boundary conditions

A detailed overview of boundary conditions specified in the simulation is given in the Table 3.2. ''Velocity inlet'' approach is used to specify inlet boundary condition of tunnel inlet and jet inlet. When performing simulating with Reynolds Stress Model, the turbulent quantities have to be imposed at inlet (i.e. inlet velocity, turbulent kinetic energy, dissipation rate and values of individual Reynolds stresses). At the tunnel inlet, uniform inlet velocity, turbulent intensity and hydraulic diameter are specified. The profile close to the pipe outlet is used as inlet boundary condition for the jet for tunnel simulation. Figure 3.4 shows fully developed velocity profile as it enters the main tunnel. The values of individual velocity components, turbulent kinetic energy, dissipation rate and individual Reynolds stresses are specified

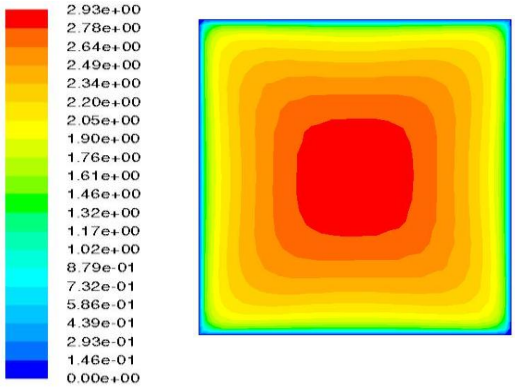

Figure 3.4: Velocity profile at inlet of jet in main tunnel

through calculated profiles at the jet inlet to the main tunnel.

On the other hand when only inlet velocity, turbulent intensity and hydraulic diameter are specified, FLUENT calculates the values of turbulent kinetic energy, dissipation rate and individual Reynolds stresses as follows:

Turbulence intensity, I, is given as

$$I = \frac{u'}{U_{avg}} = 0.16\left(Re_{D_H}\right)^{-1/8}$$

Where U_{avg} is mean flow velocity. Turbulence length scale, l, is calculated from hydraulic diameter, D_H, as

$$l = 0.07D_H$$

Turbulent kinetic energy, *k*, is calculated from turbulence intensity, *I*, as

$$k = \frac{3}{2}\left(U_{avg}\, I\right)^2$$

Turbulent dissipation rate, ε, is determined from length scale from following equation

$$\varepsilon = C_\mu^{3/4}\frac{k^{3/2}}{l}$$

For Reynolds stress components, it is assumed that turbulence is isotropic at inlet and it is calculated from turbulent kinetic energy as

$$\langle u_i u_j \rangle = 0$$

$$\langle u_\alpha u_\alpha \rangle = \frac{2}{3}k$$

(No summation over the index α) $i \neq j$ and $\alpha = 1, 2, 3$.

Table 3.2: Boundary Conditions

	Experimental Scale
Main Stream	Water
Jet Stream	Saline solution
Main Stream velocity (m/s)	0.15
Main Stream density (kg/m^3)	1000
Jet stream density (kg/m^3)	1060
Jet velocity (m/s)	2.3

CHAPTER 4

In-house Codes: Simulation Setup

When using In-house codes, the simulation is performed with standard k-ε model and modified k-ε model. The basic governing equations solved are presented in Chapter 2. The value of turbulent Schmidt number is 0.7 and Prandtl number is 609. The discretization scheme used for simulation is first order upwind scheme. In this chapter, geometry, mesh and boundary condition employed for simulation using In-house codes are presented. In the end, the implementation of density variation is explained.

4.1. Geometry

The dimensions of the tunnel geometry, made to perform simulation through In-house codes, are same as those of experimental scale tunnel. These are given in Table 1.1. The only difference is now that the length of tunnel has decreased from 4 m to 3.2 m. This is to decrease computational domain and make fine mesh. Figure 4.1 shows the geometry of the tunnel as it is built using In-house codes. An important point to note is that, when creating geometry there should be some distance between obstacles and outlet. The outlet should be away from wake formation region otherwise it will take more time to converge. This is why 0.3 m length is left after last obstacle to avoid wake formation near outlet. In the In-house codes x is in stream wise direction, y is span wise and z is in vertical direction but for the ease of the reader the results are presented with same coordinate system as it is exercised for FLUENT.

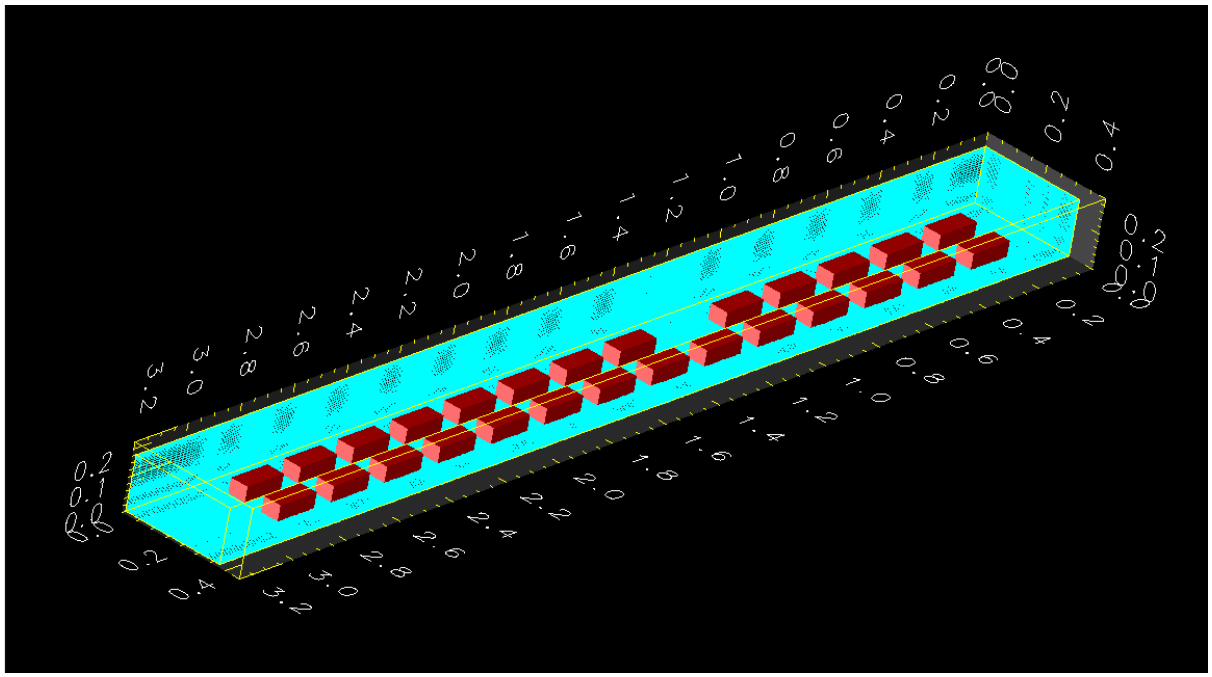

Figure 4.1: Geometry of the tunnel

4.2. Mesh

The mesh is shown in Figure 4.2 below. Two different meshes are used to perform simulation. One is course mesh containing 2.25 M cells and other is fine mesh containing 4.5 M cells. In the figure only the fine mesh is shown. The mesh is refined close to the walls and obstacles. The mesh size increases with factor of 1.12. The mesh is structured and contains hexahedral cells. Hexahedral mesh is preferred because this decreases numerical diffusion. In addition to that, very fine mesh is used for simulation to reduce numerical diffusion. Minimum cell dimensions are given in table 4.1.

Table 4.1: Mesh characteristics

Mesh	**Coarse**	**Fine**
Cells (Million)	2.25	4.5
Minimum cell length (m)	0.0025	0.0015
Minimum cell width (m)	0.0025	0.0015
Minimum cell height (m)	0.0025	0.002
Expansion faction	1.12	1.12

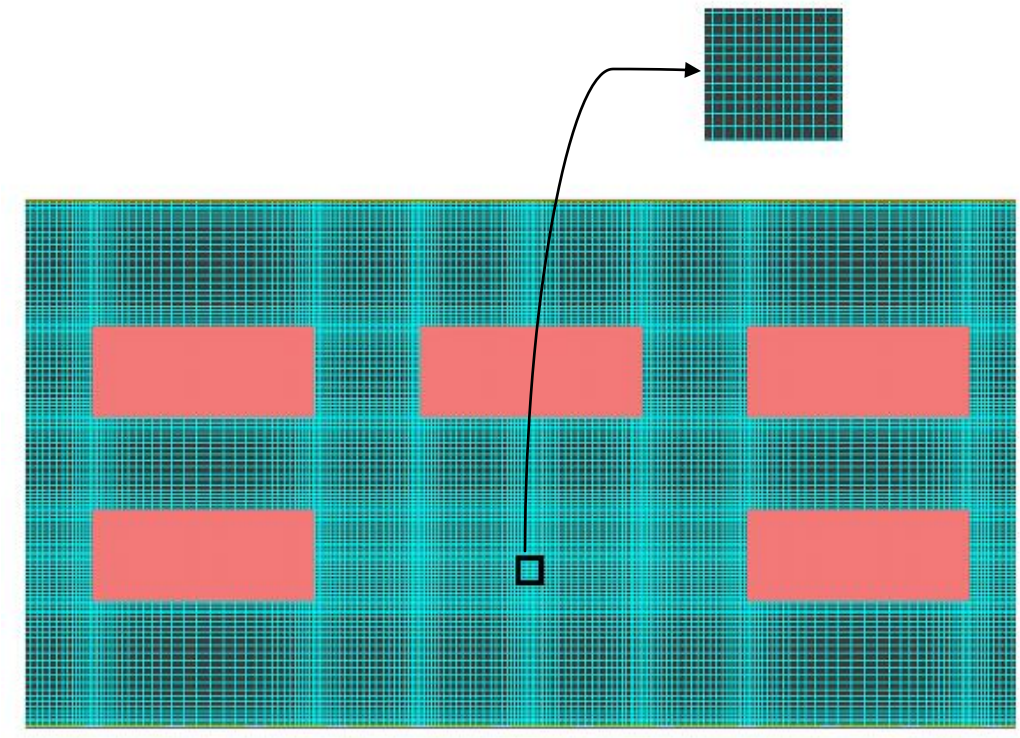

Figure 4.2: Mesh of the tunnel

4.3. Boundary conditions

The boundary conditions are given in Table 3.2. The turbulence at inflow boundaries is specified by turbulence intensity, *I*, and viscosity ratio. The turbulent intensity is given as

$$I = \frac{u'}{U_{avg}} = 0.16\left(Re_{D_H}\right)^{-1/8}$$

And viscosity ratio

$$viscosity\ ratio = \frac{\nu_t}{\nu}$$

Where

$$\nu_t = C_\mu \frac{k^2}{\varepsilon}$$

And $C_\mu = 0.09$

Appendix E includes configuration file. This file shows complete specification of boundary conditions, mesh characteristics, and solution control. The boundary condition specification for the jet is different than as it is specified in FLUENT. Velocity of the jet is specified as constant and normal to the boundary. The turbulence at boundaries is specified by turbulence intensity, *I*, and viscosity ratio. The In-house code did not allow specification of an inlet profile as done with FLUENT.

4.4. Density variation implementation

The option to specify different density for different inlet streams, at the start of the project, was not available with In-house code. This variation of density has been implemented in codes during the project. For a computational cell the density is calculated as a function of scalar fraction.

$$\rho = \rho_1(1 - Y) + \rho_2 Y$$

Where *Y* is the scalar faction varying from 0 to 1, ρ_1 is the density of the mainstream and ρ_2 is the density of the jet material.

It has been identified that the term ρg_i in the Navier-Stokes equation is an important term when streams have different densities. This term is responsible for heavy fluid to feel gravity and move down. This term is implemented in the codes. The FORTRAN codes written are given in Appendix D.

The Figure B2 and B3 in Appendix B show how the scalar is dispersed if the effect of gravity is neglected. These plots should be compared with Figure B4 and B5. In the contour plots given in Figure B4 and B5

the effect of gravity is implemented. The comparison shows that if the gravity is not included the jet material flows to the ceiling and does not come down even though it has higher density. This effect is not physical and contours shown in Figure B4 and B5 show that the jet material with higher density feels the bouncy force and moves down. In Figure B4 a) and b) we can see how the jet material is moving down and the jet material is located close to floor at the end of the tunnel. Thus the density implementation is successful.

CHAPTER 5

Result Validation

In this chapter, simulation results are validated through measurements. The available measurement data is based on U velocity (velocity in x direction), V velocity (velocity in y direction), turbulent kinetic energy, *k*, and *uv* Reynolds stress. Values of these parameters are available along the x direction, at different span wise positions (in z direction) and at different heights (in y direction). Mainly measurements are taken at z equal to 0.056m and 0.104m. The jet inlet is at z = 0.056m. In y direction measurements are taken at y/h equal to 0.5, 0.8, 1.2 and 1.5. Where h is the height of obstacles and h = 0.049 m. In x direction measurements start at x equal to 1.2 m and these are taken up to x = 1.82 m. The jet inlet is at x = 1.218 m. The location of the measurements can be seen in Figure C1 and C2 in Appendix C. Two figures show top and side view of tunnel and the locations of the available measurement. In the analysis, the region close to the jet is studied and results from simulation and experimental measurements are compared. Measurements are compared with the results obtained by Reynolds stress model and standard *k-ε*. The results obtained after Durbin model modification in standard *k-ε* did not show any significant difference this is why the results of modified *k-ε* model are not presented.

5.1. U velocity

Figure 5.1 shows the U velocity plot against x coordinate, at z = 0.056m and at different heights. Figure on the right shows the location of plot. The results from both, the simulations and the measurements, are presented on the same plot. Plot shows nice agreement between simulations and experimental results. It can be seen that the rise and fall of U velocity is nicely predicted by both models (standard *k-ε* (RANS) and Reynolds stress model (RSM)). In the plot at y/h = 1.5, 0.8 and 0.5 simulation results resemble with experimental results to great extent. Note that, in the plot at y/h = 0.5, U velocity has negative values in between the obstacles. This is because of wake formation which can be seen in Figure 6.4 which shows velocity vector contour. This effect is clear in both experimental and simulation results.

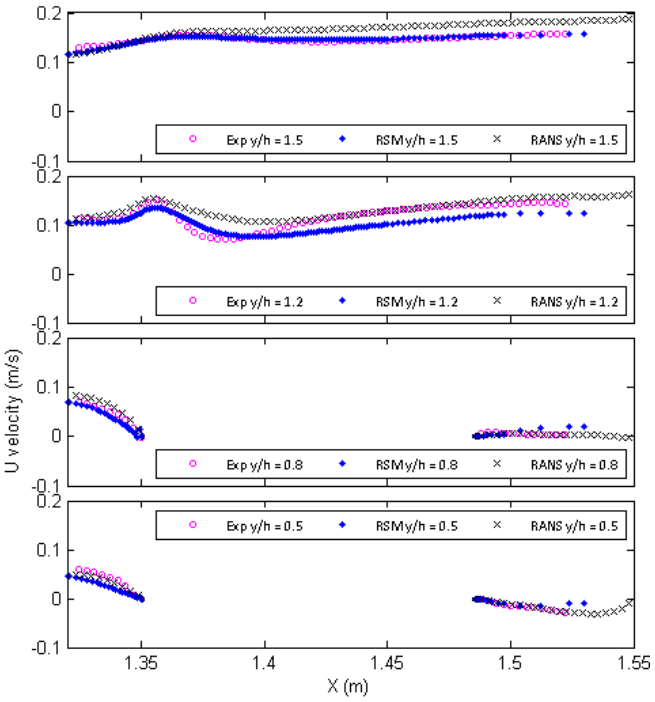

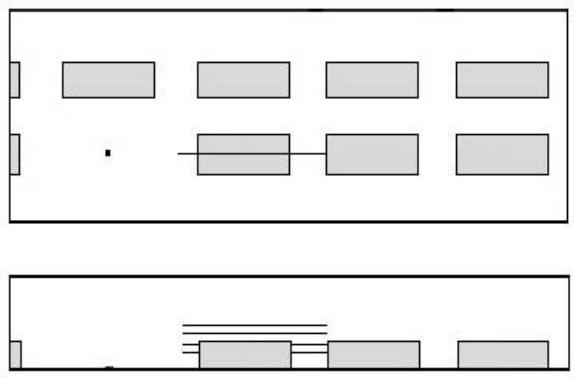

Top and side view of tunnel. The lines indicates the location of plot on the left.

Figure 5.1: U velocity at z = 0.056

More plots of U velocity at different locations are included in Appendix A1. It can be seen in the plots that, at some locations Reynolds stress model shows better agreement with measurements and at some locations *k-ε* model shows better agreement. However, the pattern and peaks predicted by the model is in agreement with experimental results.

5.2. V velocity

Analogous to U velocity, results of V velocity (velocity in y direction) from simulation are validated through measurements. Figure 5.2 shows V velocity plotted against x coordinates, starting from x = 1.33m and at z = 0.056m. Similar to U velocity, V velocity is also nicely predicted by both the models. It can be seen, in plot at y/h = 1.2, that the V velocity is high at x = 1.35. This is the location of the first obstacle after the jet. Due to the presence of the obstacle, the V velocity has increased at this location. Note that the velocity values between the obstacles are varying from positive value to negative values. This shows the presence of the wake in between obstacles. This effect is also captured by both models and result is validated through the measurements. The values of V velocity in this region are almost identical to experimental results. This is a good validation of both models. It can be stated that these models are predicting the region between the obstacles quite effectively. In the plot at y/h = 1.5 and at x = 1.34 *k-ε* show better agreement with measurements as compare to RSM. On other location no significant difference is observed.

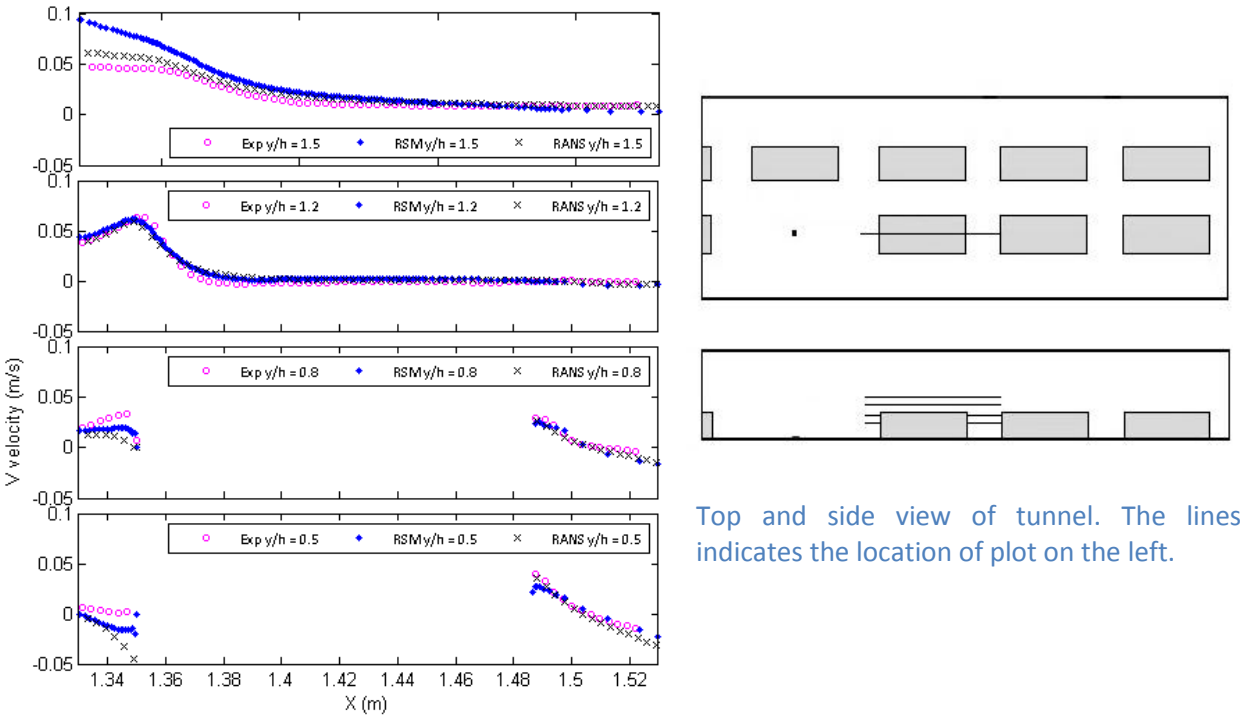

Figure 5.2: V velocity at z =0.056

Appendix A2 shows more V velocity plots at different locations. The values of V velocities are very small since the flow is mainly in x direction. Model results of V velocity are quite close to measurements. However, this is not true everywhere. For instance in Figure V2, it can be seen that simulation and experimental results shows some disagreement.

5.3. Turbulent kinetic energy, *k*

Figure 5.3 shows turbulent kinetic energy plotted against x coordinates at z = 0.056 and at different heights. The values of turbulent kinetic energy predicted by the models are of the same order of magnitude as given by the measurements. Plot at y/h = 1.5 shows much resemblance. Also values of turbulent kinetic energy in between obstacles determined by the models shows much agreement with measurements. On the other hand, in the plot at y/h = 1.2 and at x = 1.37 significant difference is seen. The values of turbulent kinetic energy, as predicted by both the models, do not show a high peak just above the obstacle as given by the measurements. Here Reynolds stress model shows better result as compared to *k-ε* model. More plots of turbulent kinetic energy at different locations are presented in the Appendix A3.

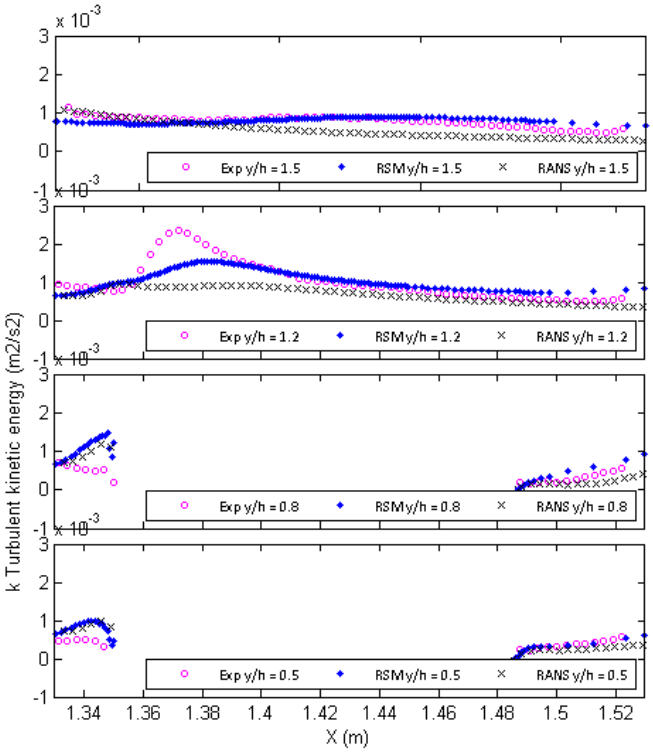

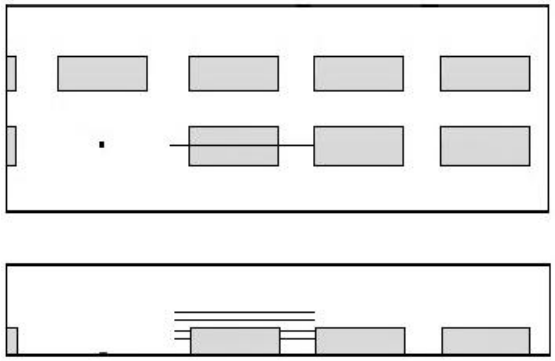

Top and side view of tunnel. The lines indicates the location of plot on the left

Figure 5.3: Turbulent kinetic energy at z = 0.056

5.4. Reynolds Stress, *uv*

Figure 5.4 shows the plots of *uv* Reynolds stress against x coordinates at z = 0.056 m. In the plot, the Reynolds stress, as predicted by the model, is compared with the measurements. Here the measurements are only compared with results of Reynolds stress model. The Reynolds stresses are very small quantities typically of the order of $10^{-4}m^2/s^2$. Unlike to the velocities, the simulation results of Reynolds stress show significant disagreement with measurements at y/h = 1.2. However in between obstacles there is close agreement. More plots of Reynolds stress at different locations are presented in the Appendix A4.

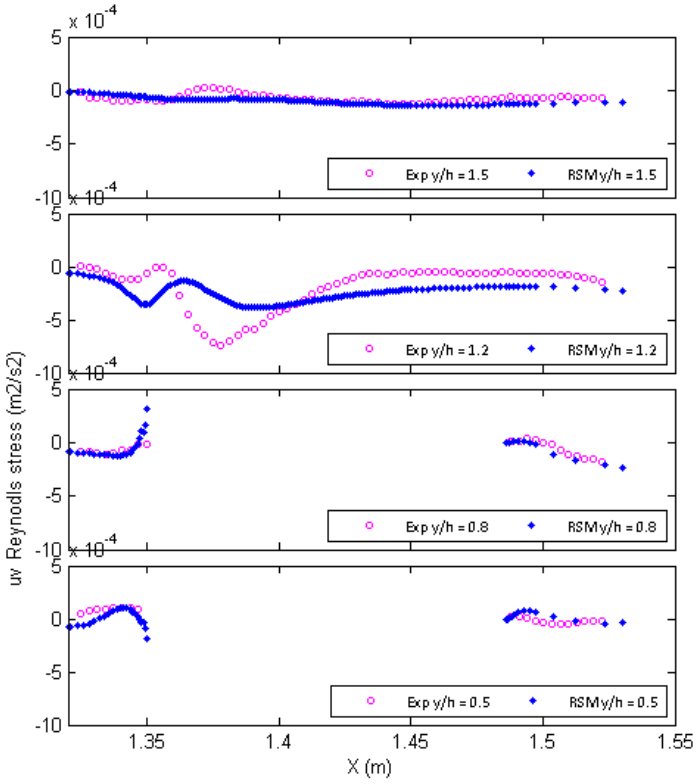

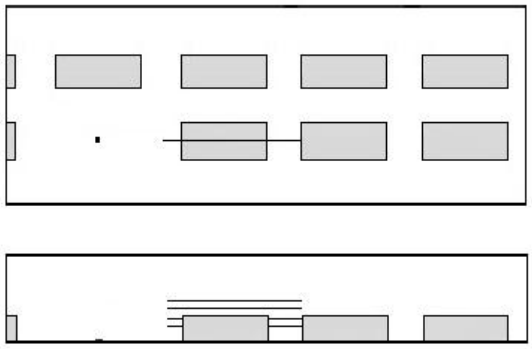

Top and side view of tunnel. The lines indicates the location of plot on the left.

Figure 5.4: u'v' Reynolds Stress at z = 0.056

CHAPTER 6

RESULTS

In this section results obtained from Reynolds stress model are discussed. Different features of the flow are analyzed and these are compared with literature. For near wall modeling ''Enhanced wall treatment'' approach is employed. The scalar dispersion results obtained by In-house codes are not presented because the In-house codes require some modifications which have been suggested during this study. Simulation performed with Standard k-ε and modified k-ε models using In-house codes will serve as bases for further studies.

6.1. Results and Discussion

As discussed earlier, in the literature review, one of the important features of the jet in cross-flow (JICF) is the counter rotating vortex pair (CRVP) which is formed at some distance from the jet inlet. This CRVP is found in many studies carried out on the jet in cross-flow (Plesniak 2005). This CRVP is also seen in the simulation results. Figure 6.1 shows the contour plot of the vorticity magnitude captured at some distance from the jet inlet (at x = 1.3 m). It shows that two counter rotating vortexes are produced away from the jet. Similarly, another important feature of JICF is formation of ''horse shoe vortex'' near the jet inlet. This horse shoe vortex is also seen in the simulation results and it is presented in Figure 6.2. These interesting results show that Reynolds stress model resolves the main structure of the velocity field of the JICF quite efficiently and it predicts important feature of the jet nicely.

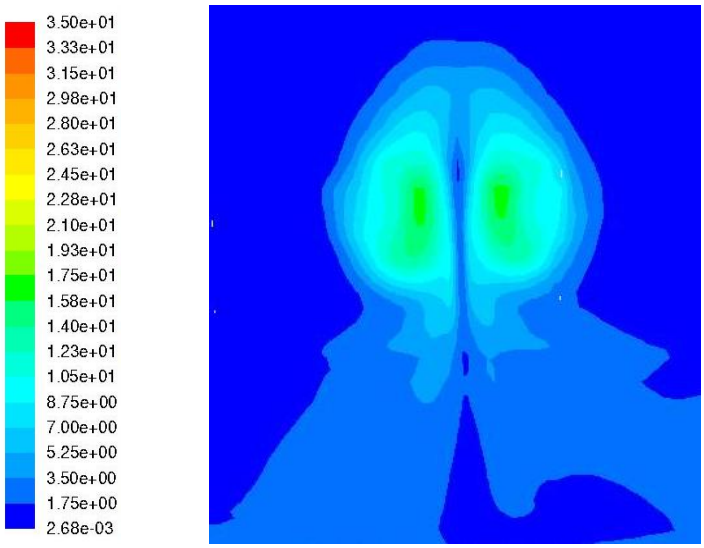

Figure 6.1: Vorticity magnitude (1/s) contour at x = 1.3

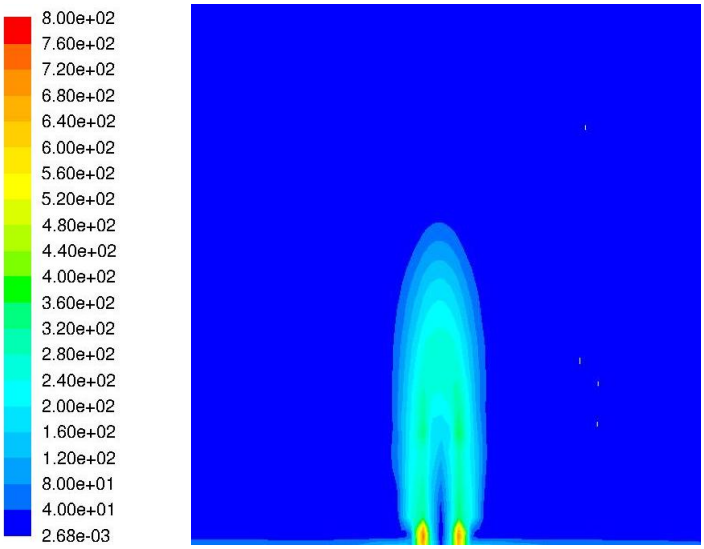

Figure 6.2: Vorticity magnitude (1/s) contour at x = 1.218

The vector plot presented in Figure 6.3 shows how the flow is affected by the presence of obstacles. In between obstacles there is a low velocity region and wake formation. Figure shows velocity vector between obstacles. It can be seen that wake has been formed between the obstacles. This wake formation is also validated through experimental results. These results are presented in the result validation section.

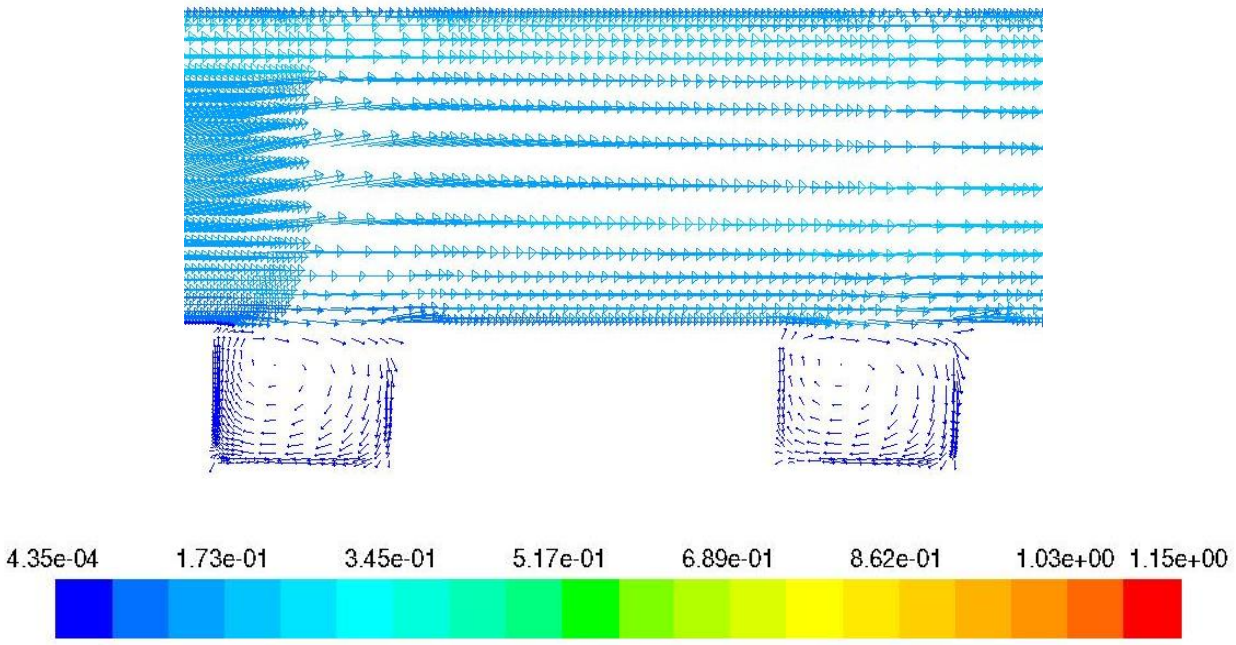

Figure 6.3: Velocity vectors colored by velocity magnitude (m/s)

6.2. Scalar Dispersion

The most obvious characteristic of the jet in cross-flow is that the jet bends and aligns itself with the cross-flow. This behavior of jet is visible in Figure 6.4. Figure 6.4 and 6.5 present contour plots of scalar fraction. Contours are taken at different location. The Figure C3 in the Appendix C shows the location at which these contours are obtained. Figure 6.4 and 6.5 show how scalar is dispersed in the tunnel. The scalar is injected in vertical direction, through the opening in the floor and it reaches near the ceiling. Initially the scalar is located close to the ceiling of the tunnel. Then it slowly moves down as going downstream. Close to tunnel exit most of scalar is located near the floor. This effect is realistic and proven by literature study. The jet material has higher density ($\rho_j = 1060\ kg/m^3$) than the main stream ($\rho = 998\ kg/m^3$) so it is moving down slowly and converging close to the floor. In the report of Kevin Gosse (2009) it was also found that scalar was located near the floor. In the top view of the tunnel, it is analyzed that the jet material has not dispersed throughout the cross-section of the tunnel. However as going downstream the jet material has dispersed throughout the cross-section and close to the floor of the tunnel.

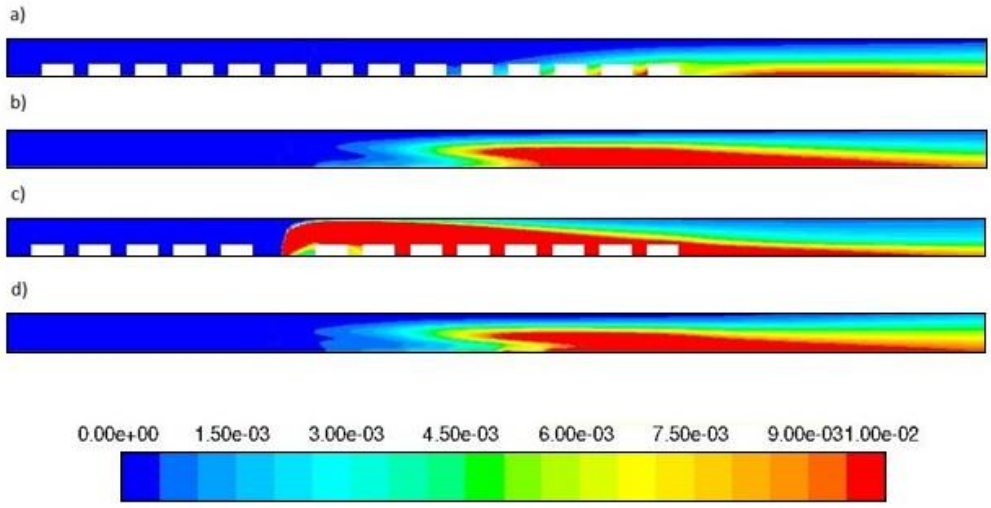

Figure 6.4: Concentration Contour at, a) z = -0.056m, b) z = 0, c) z = 0.056m, d) z = 0.104m

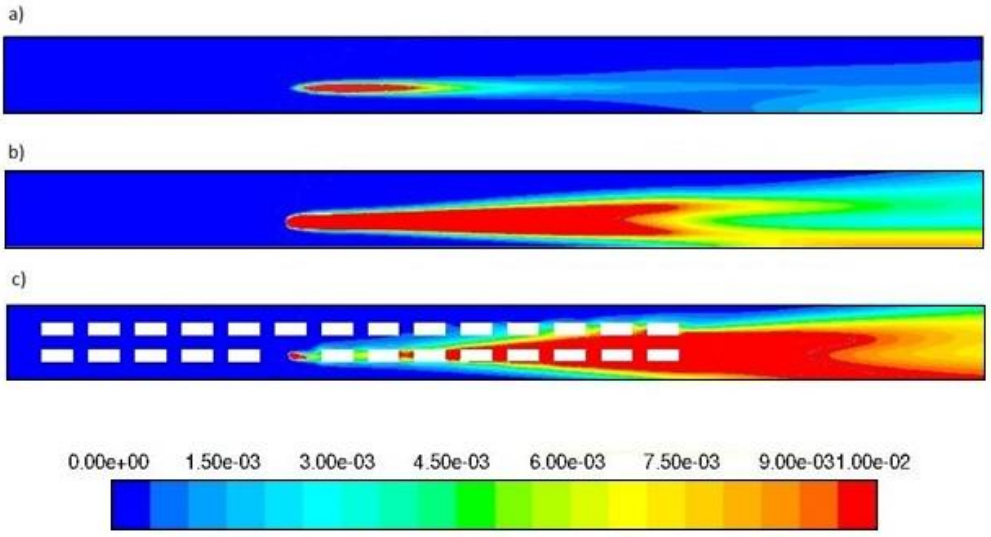

Figure 6.5: Concentration Contour at, a) y = 0.0245m, b) y = 0.0735m, c) y = 0.14m

6.2.1. Flammable region

As explained in the scaling rules, the real tunnel is scaled down to experimental scale tunnel with constant I_{ratio} but Vol_{ratio} is not constant. This means that, the lower flammability limit (LFL) and the upper flammability limit (UFL) has to be calculated for experimental scale tunnel. We can estimate the flammable region for the experimental case from the hypothesis:

$$\frac{(Vol\ \%)_{real}}{(Vol\ \%)_{exp}} = \frac{(Flammability\ limit)_{real}}{(Flammability\ limit)_{exp}}$$

Where

$$Vol\ \% = \frac{U_{jet}\, A_{jet}}{U_{flow}\, A_{flow} + U_{jet}\, A_{jet}}$$

The flammability limit of LPG/air mixture and corresponding experimental scale limits are given in Table 6.1 (Mishra 2002).

Table 6.1: Flammability limits

	Experimental case	**Real case (LPG/air)**
I_{ratio}	250	250
$Vol\ \%$	0.0074	0.0057
Lower flammability limit (*Vol%*)	2.4	1.8
Upper flammability limit (*Vol%*)	11.4	8.7

The Figure 6.6 shows the region in which volume percentage of saline solution/water (and corresponding LPG/air) mixture is in LFL and UFL. This is the region where the volume percentage of LPG is such that it will make stable flame if a source of ignition is found. The flammable region is only made close to the source and along the jet. Although the scalar is disperse throughout the tunnel but the flammable region is only made close to source and until 5 pair of obstacles.

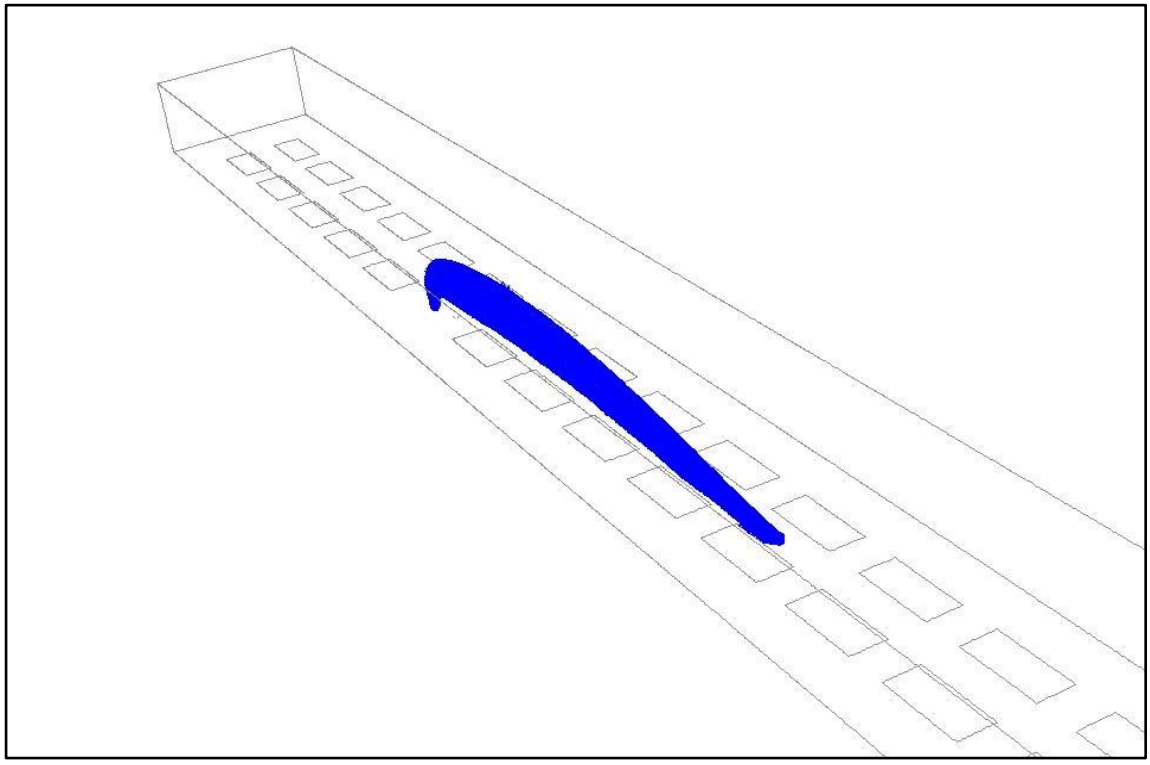

Figure 6.6: Iso surface of scalar volume percentage at LFL

6.3. Turbulent kinetic energy

Figure 6.7 shows a contour plot of turbulent kinetic energy, *k*, passing through the jet inlet. The contour shows high values of turbulent kinetic energy at the location of the jet. Note that the turbulent kinetic energy is high where main stream interacts with the jet. This important feature is according to the expectations. This is region where there is maximum gradient in the velocity that is why turbulent kinetic energy is high in this region. This is nicely predicted by the model. These results became visible when the mesh close to the jet was refined. It is revealed that refining the mesh captures small features of the flow which can contribute to improvement of results to great extent.

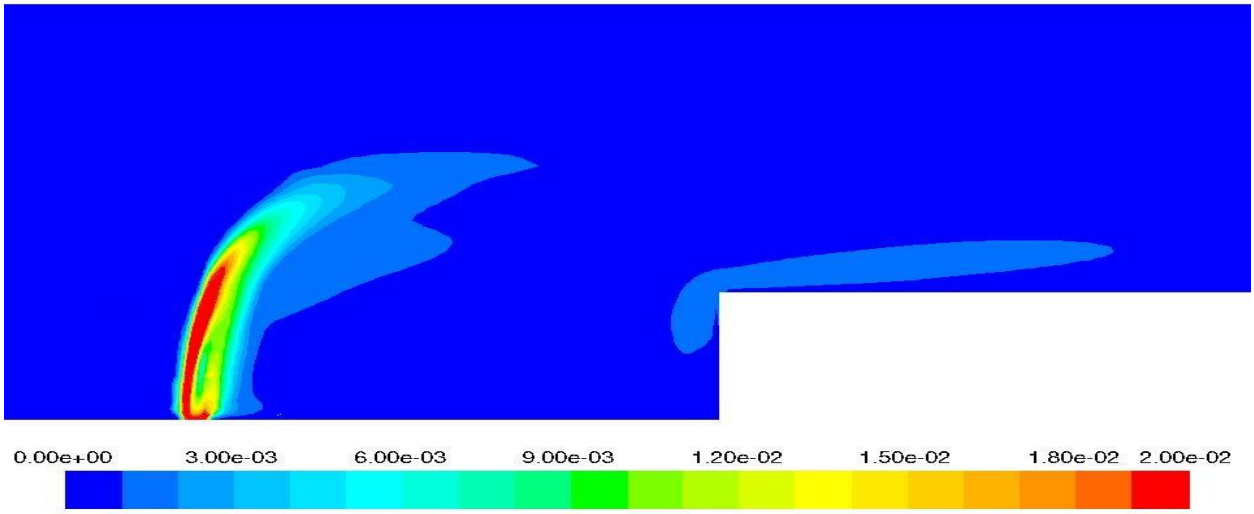

Figure 6.7: Contour of Turbulent kinetic energy (m^2/s^2)

6.4. Conclusions

From the analysis of simulation results it can be concluded that the Reynolds stress model has predicted jet in cross-flow (JICF) quite accurately. The features of the jet as captured from simulation are exactly according to the literature results on the jet in cross-flow. Simulations predictions of 'Horse Shoe Vortex' and 'Counter rotating vortex pair' are important features of JICF.

Simulation results are validated through measurements. Close agreements between simulation and experimental results are seen at many locations. However, there are disagreements as well. Especially disagreement is seen in turbulent kinetic energy and Reynolds stress. The model has nicely predicted wake formation between the obstacles and these results are validated through measurements. It can be concluded that the model is quite effective in predicting region between the obstacles. This accuracy of results is obtained after making some improvements in the simulations. These improvements are

1. Grid refinement to obtain completely grid independent solution.
2. Fully developed profile is used for jet injection. This is exactly in accordance to experimental setup.
3. Enhanced wall treatment approach is used to model near wall region.

CHAPTER 7

GENERALIZATION

In this chapter, simulation results for two different cases are presented. In one case simulation is performed with low jet density ($\rho_{jet} = 925\ kg/m^3$) while in other case simulation is performed with low jet velocity $v_{jet} = 1.15\ m/s$. These cases are simulated using Reynolds stress turbulence model and for near wall modeling Enhanced wall treatment approach is used. These cases are included to analyze the effect of density and velocity ratios on jet features and scalar dispersion.

7.1. Simulation for the case of H_2

Simulation for the case of hydrogen is performed using Reynolds stress turbulence model. The near wall modeling is done using Enhanced wall treatment. This model setting is being used because it has already been tested and validated through measurements and literature. The simulation for the case of Hydrogen is performed with the experimental scale tunnel. This is to compare with experimental scale LPG case and analyze the importance of density ratio. The boundary conditions used are given in Table 7.1 and corresponding real tunnel specifications are also given for comparison. Here the water is used as main stream (with $\rho = 998\ kg/m^3$ and velocity $U_\infty = 0.15\ m/s$) and light liquid is used as jet (with $\rho_j = 927\ kg/m^3$ and velocity $U_j = 2.3\ m/s$). The case of hydrogen is scaled down from real tunnel in the same way as the scaling was done in the case of LPG. Different scaling parameters are considered. These are Richardson number, *Ri*, velocity ratio, v_r, and I_{ratio}. In this case density ratio ($\rho_{ratio} = \rho_{jet}/\rho_{cf} = 0.927$) is different than the case of LPG ($\rho_{ratio} = 1.06$).

Figure 7.1 and 7.2 shows the contour plot of scalar fraction at different location. If we compare the contour plots with the contours presented in Figure 6.4 and 6.5, we can detect significant difference. Here the jet being light liquid reaches the ceiling. This result is realistic since jet liquid has low density as compare to main stream so it experiences upward buoyant force. This result shows that for the real case, when H2 is leaked inside the tunnel it will flow to the ceiling. Table 7.1 also shows the flammability limits of hydrogen/air mixture and corresponding volume percentage in the case of light liquid/water. The Figure B7 given in Appendix B shows the flammable cloud formed in the tunnel in case of leakage of Hydrogen. The flammable region is close to the ceiling and it persists far downstream as compared to the case of LPG/air.

Table 7.1: Boundary conditions

	Simulation Case	**Full Scale**
Main Stream	Water	Air
Jet Stream	Light solution	Hydrogen
Main Stream velocity (m/s)	0.15	3
Main Stream density (kg/m^3)	1000	1.205
Jet stream density (kg/m^3)	925	0.083
Jet velocity (m/s)	2.3	165.7
I_{ratio}	217	217
Vol_{ratio}	0.0075	0.027
LFL (*Vol %*)	1	4
UFL (*Vol %*)	20	75

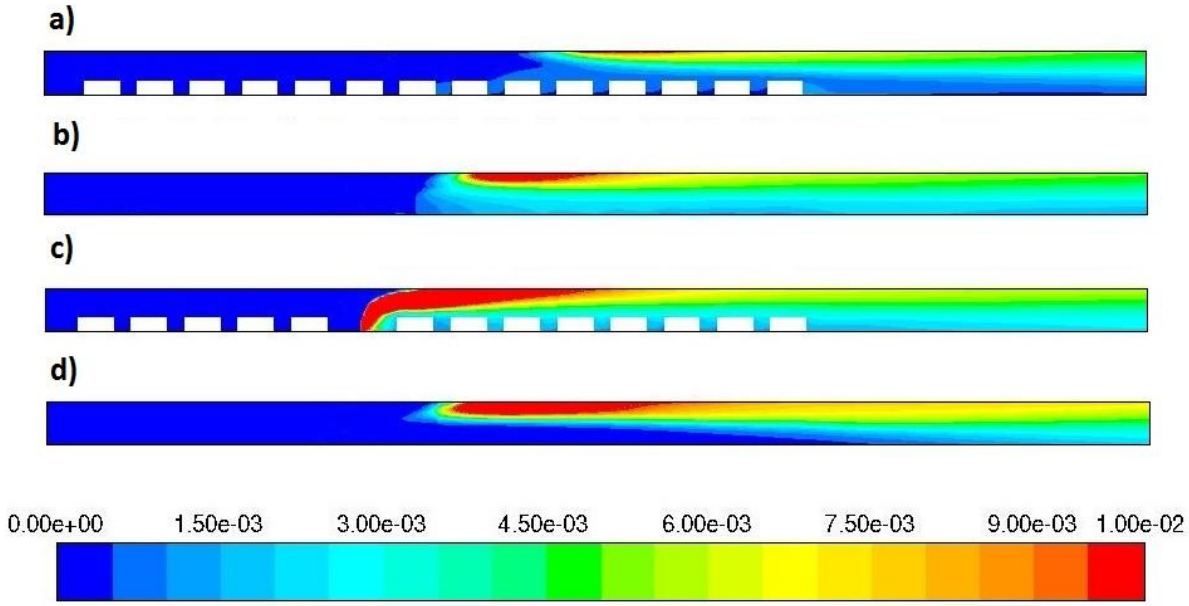

Figure 7.1: Concentration Contour at, a) z = -0.056m, b) z = 0, c) z = 0.056m, d) z = 0.104m

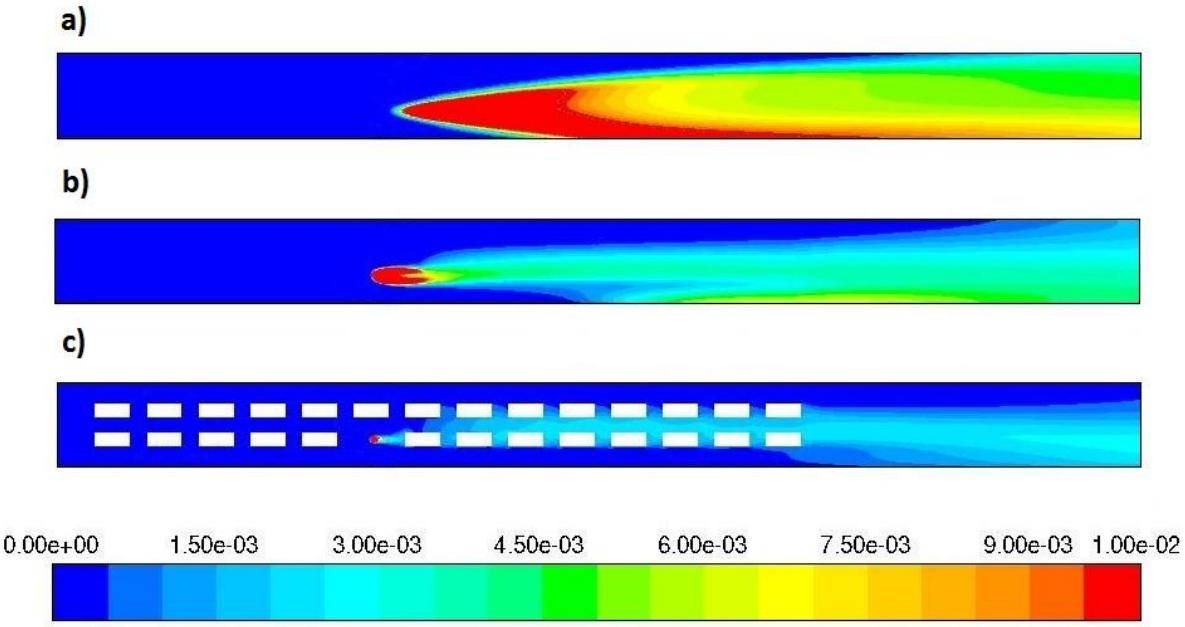

Figure 7.2: Concentration Contour at, a) y = 0.0245m, b) y = 0.0735m, c) y = 0.14m

7.2. Different velocity ratio case

In this case, the importance of velocity ratio has been investigated. The simulation is performed with low jet velocity keeping the main stream velocity constant. The boundary conditions used for simulation are given in Table 7.2. Analogous real tunnel specifications are also included in the Table 7.2.

Table 7.2: Boundary conditions

	Simulation Case	**Full Scale**
Main Stream	Water	Air
Jet Stream	Saline solution	LPG
Main Stream velocity (m/s)	0.15	3
Main Stream density (kg/m^3)	1000	1.205
Jet stream density (kg/m^3)	1060	2.175
Case	**Low jet velocity**	**Low jet velocity**
Jet velocity (m/s)	1.15	17.6

Contours presented in Figure 7.3 and 7.4 shows how scalar is dispersed for the case of low jet velocity. It can be seen that jet has not gone much in vertical direction and it has bended along the stream wise direction. The jet has not reached near the ceiling, so all the jet fluid is located near the floor. This result was also deducted during the experimental investigation of Kevin Gosse (2009). According to his report, for the case of low jet velocity the scalar field is localized close to the ground floor and on the injection side of the channel, outside the wake zone of the obstacles. This is an important observation. This shows that the velocity ratio is an important parameter for scalar dispersion and jet features.

Figure B6 in Appendix B shows the flammable region of LPG/air mixture when jet velocity is low. It can be seen that flammable region is close to the floor and in between the pairs of obstacle, not in the wake region. Flammable region is also located between jet side wall and obstacles.

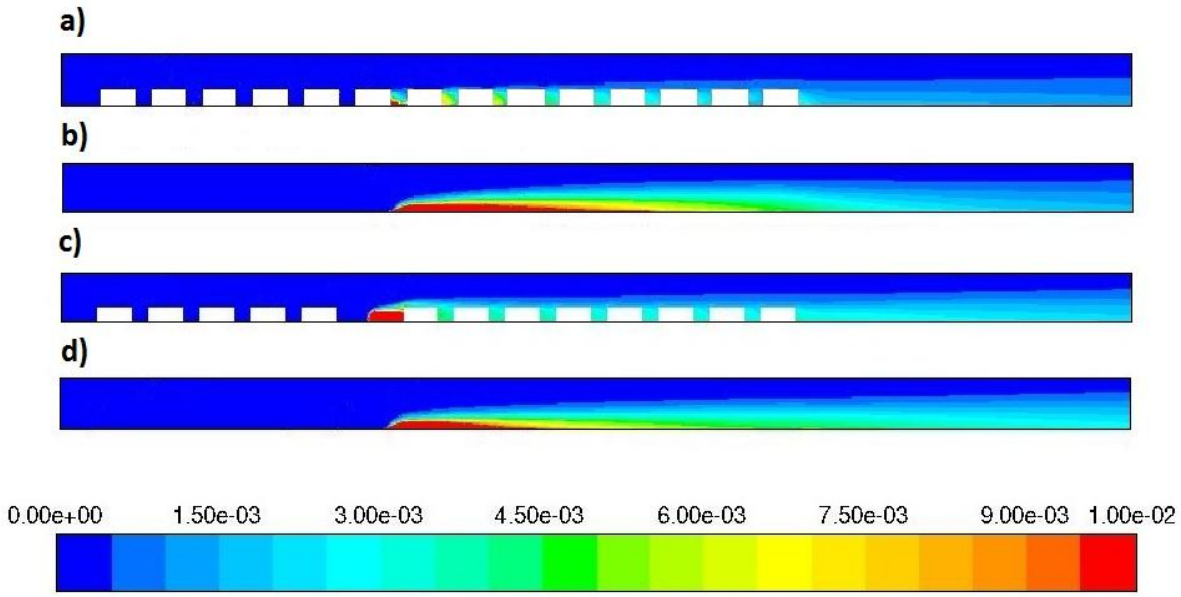

Figure 7.3: Concentration Contour at, a) z = -0.056m, b) z = 0, c) z = 0.056m, d) z = 0.104m

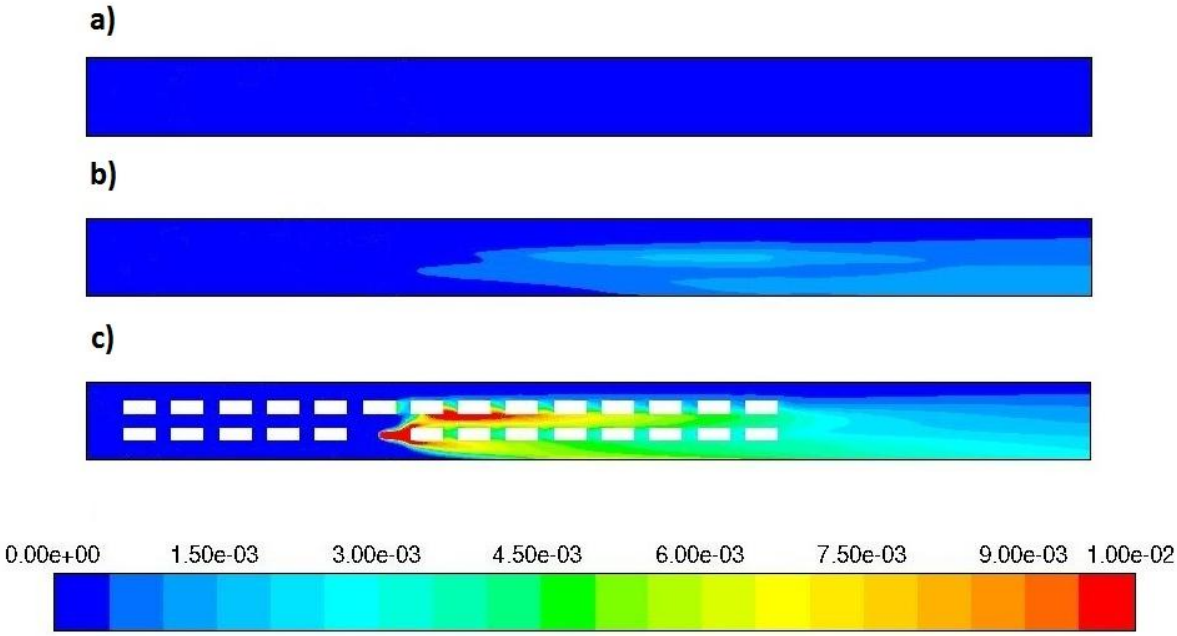

Figure 7.4: Concentration Contour at, a) y = 0.0245m, b) y = 0.0735m, c) y = 0.14m

Final Conclusions and Recommendations

The following conclusions can be drawn from this computational study:

- Reynolds stress model has predicted important features of jet quite efficiently. Horse shoe vortex (HSV) and counter rotating vortex pair (CRVP) has been predicted nicely.

- The turbulence kinetic energy close to jet is predicted and wake formation region between obstacles are predicted efficiently by both models i.e. Reynolds stress model and standard k-ε.

- Reynolds stress model, standard k-ε and modified k-ε model shows close agreement with measurements for U and V velocity. Close agreement with measurement for turbulent kinetic energy is also observed at many locations.

- No significant improvement is observed by ''Durbin time scale limiter'' modification.

- Refining the mesh is important to capture small feature of the flow.

- Using a profile for jet inlet profile is important to obtain correct jet development.

- Density ratio and velocity ratio are important parameters for JICF and scalar dispersion.

- Flammable region is found close to the jet for the case of LPG/air and it persists far downstream for the case of hydrogen/air mixture.

The following are the recommendations for the improvement of the approach:

- Model improvement should be done to better predict turbulent kinetic energy.

- Scalar fraction, as predicted by the models, should also be compared with scalar measurements.

- Simulation using In-house code is more time consuming as compare to FLUENT. Work on In-house codes should be done to obtain fast convergence.

- Parallel processing is not available in In-house code this should be implemented to obtain fast convergence.

Further studies

Hybrid T-RANS/LES simulation can be done using In-house code to obtain better results, if required. Case files for Hybrid T-RANS/LES simulation has been made and can be used for further studies.

Large eddy simulation can also be performed using FLUENT. For LES it is not advised to use full domain of the tunnel as it is now. This will make LES case computationally very expensive. A velocity profile, few obstacles upstream, can be saved in FLUENT, which can be used as inlet boundary condition for LES. As a rule of thumb the large eddy is approximately has the size of one tenth of the characteristic dimension of the tunnel. And around 30 to 50 cells should be given to resolve the large eddy. The cell dimension for LES will be around 1 mm. It is advised to have fine mesh where there is high gradient. LES requires the simulation to be done with time step size very small. Time simulation should be performed for few residence times.

Experiments with low jet velocity ($v_{jet} = 1.15\ m/s$) are performed but results are not published jet. When those results will be available they can be compared with already available simulation results in section of low jet velocity case for validation.

Concentration measurement should be available to compare the results of scalar dispersion.

References

1. Andersson, B., Andersson, R., Håkansson, L., Mortensen, M., Studiyo, R., and Berend van Wachem. 2010. *Computational Fluid Dynamics for Chemical Engineers.* 6th Edition. Gothenburg, Sweden.

2. Brungart, T.A., Petrie, H.L., Harbison, W.L., and Merkle, C. L. 1991. *A fluorescence technique for measurement of slot injected fluid concentration profiles in a turbulent boundary layer.* (Experiment in fluids 11: pp. 9-16)

3. Busking, T. 2010. *Numerical Simulation of Transient Effects in Turbulent Dispersion of Pollutants in Simplified Urban Areas at Laboratory Scale.* Master's Thesis. Delft University of Technology.

4. Ciambelli, P., Bucciero, A., Maremonti, M., Salzano, E., and Maselllis, M. 1997. *The risk of transportation of dangerous goods: BLEVE in a tunnel.* Annals of Burns and Fire Disasters – vol. X – n. 4. Italy, Naples, Palermo.

5. FLUENT 6.3: User's guide. 2006. FLUENT int., NH, USA.

6. Hai-Lang, Z., and Shi-Jun, H. 1996. *Viscosity and density of water + sodium chloride +potassium chloride solution at 298.15K.* (Journal of chemical engineering data 41: pp. 516-520)

7. Hanjalic, K. and Kenjeres, S., 2008. *Some development in turbulence modeling for wind and environmental engineering.* Delft University of Technology, Netherlands: Journal of Wind Engineering and Industrial Aerodynamics.

8. Hunt, A., and Castro, I. P. 1984. *Scalar dispersion in model building wakes.* (Journal of wind engineering and industrial aerodynamics 17: pp. 97-118)

9. Gambit 2.2 Tutorial Guide. 2004

10. Gosse, K., Tummers, M., and, Roekaerts, D. 2009. *Concentration measurement in an experimental model system for a release of LPG in a road tunnel with obstacles.* Netherlands: Department of Multi-scale Physics, Delft University of Technology.

11. Verdoold, J., Tummers, M., and, Roekaerts, D. *Velocity field measurement in an experimental model system for a release of LPG in a road tunnel with obstacles.* Netherlands: Department of Multi-scale Physics, Delft University of Technology, (in preparation)

12. Kenjeres, S., and Hanjalic, K. 2006. *LES, T-RANS and hybrid simulations of thermal convection at high Ra numbers.* Netherlands: International Journal of Heat and Fluid Flow.

13. Hanjalic, K., Kenjeres, S., Tummers, M.J., and Jonker, H.J.J. 2007. Analysis and Modelling of Physical Transport Phenomena. VSSD, Delft.

14. Huang, P., Bradshaw, P., and Coakley, T. 1993. *Skin Friction and Velocity Profile Family for Compressible Turbulent Boundary Layers.* AIAA Journal, 31(9):1600-1604.

15. Gibson, M. M., and Launder, B. E. 1978. *Ground Effects on Pressure Fluctuations in the Atmospheric Boundary Layer.* J. Fluid Mech, 86, pp-491-511.

16. Mishra, D. P., and Rahman, A., 2002. *An experimental study of flammability limits of LPG/air mixtures.* India.

17. Perry, R. H., and Green, D. W. 1997. *Perry's Chemical Engineering' Handbook (7th Edition).* McGraw-Hill.

18. Plesniak, M.W., and Cusano, D.M. 2005. *Scalar mixing in confined rectangular jet in crossflow.*United Kingdom: Cambridge University Press. (J. Fluid Mech. (2005), vol. 524, pp. 1-45).

19. Pope, S. B. 2000. *Turbulent Flows.* United Kingdom: Cambridge University Press.

20. Ramezanizadeh, M., Taeibi-Rahni, M., and Saidi, M.H. 2007. *Investigation of density ratio effects on normally injected cold jets into a hot cross flow.* Springer-Verlag. (Arch Appl Mech (2001) 77: pp. 835-847)

21. Roekaerts, D. *Note on scaling of measured concentration profiles.* TU Delft.

22. Roekaerts, D. *Presentation on Scaling of dispersion experiment.* TU Delft.

23. Smith, S. H., and Mungal, M. G. 1998. *Mixing, structure and scaling of the jet in crossflow.* United Kingdom: Cambridge University Press. (J. Fluid Mech. (1998), vol. 357, pp. 83-122).

24. Trijssenaar-Buhre, I.J.M., Van der Welle, P., and Wijnant-Timmerman, S.I. 2009. *Dispersion of LPG in a road tunnel – Results of CFD simulation in CFX and Ventunnel.* Netherlands: TNO

25. Wegner, B., Huai, Y., and Sadiki, A. 2004. *Comparative study of turbulent mixing in jet in cross-flow configurations using LES.* Germany: International Journal of Heat and Fluid Flow.

26. White, F., and Christoph, G. 1971. *A Simple New Analysis of Compressible Turbulent Skin Friction Under Arbitrary Conditions.* Technical Report AFFDL-TR-70-133.

27. Wolfstein, M. 1969. *The Velocity and Temperature Distribution of One-Dimensional Flow with Turbulence Augmentation and Pressure Gradient*. Int. J. Heat Mass Transfer, 12:301-318.

Appendix

Appendix

Appendix A1: U velocity plots at different x and z locations

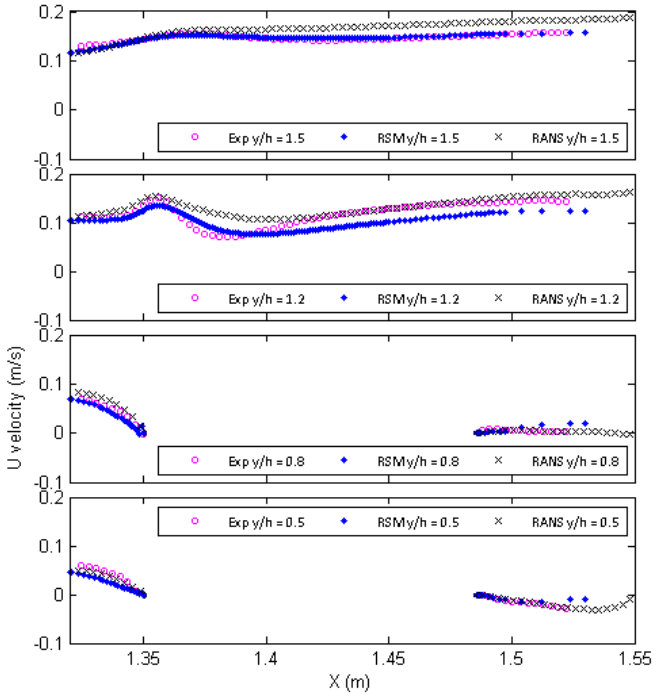

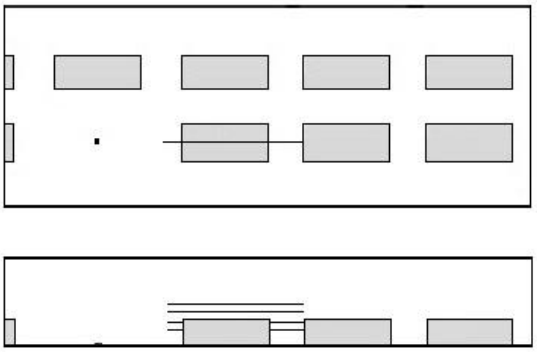

Top and side view of tunnel. Lines indicates the location of the plot on the left.

Figure U1: U velocity at z = 0.056

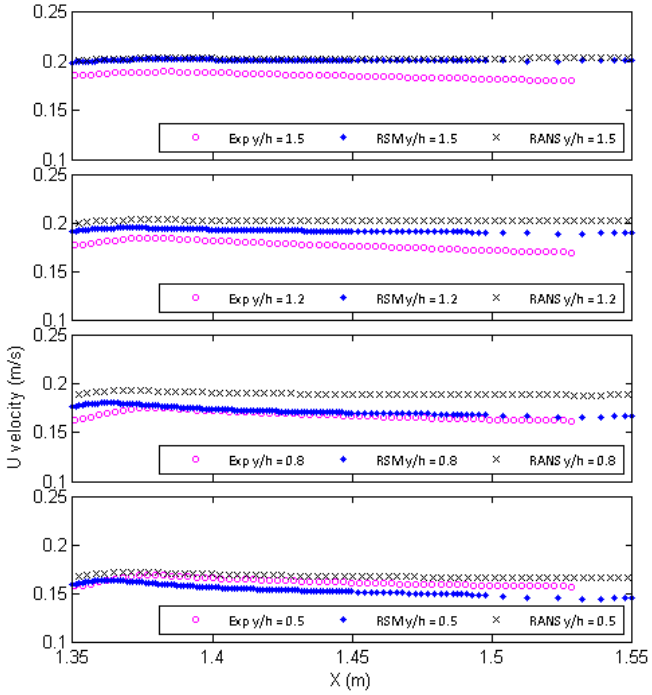

Top and side view of tunnel. Lines indicates the location of the plot on the left.

Figure U2: U velocity at z = 0.104

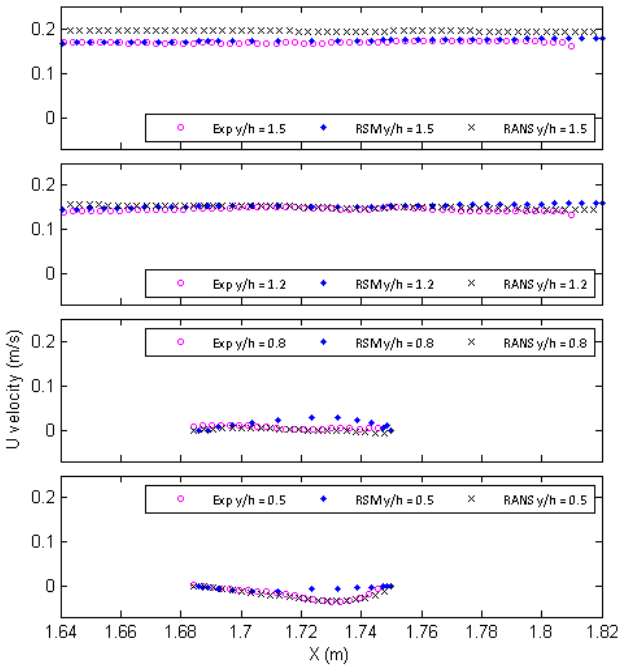

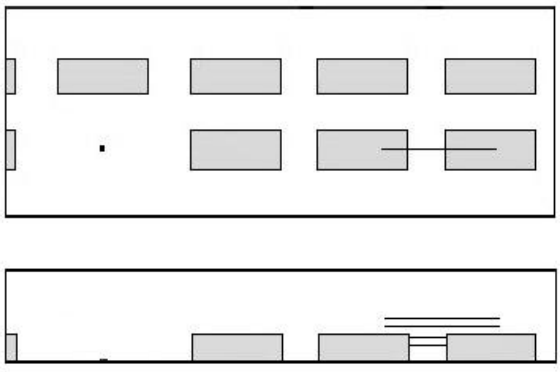

Top and side view of tunnel. Lines indicates the location of the plot on the left.

Figure U3: U velocity at z = 0.056

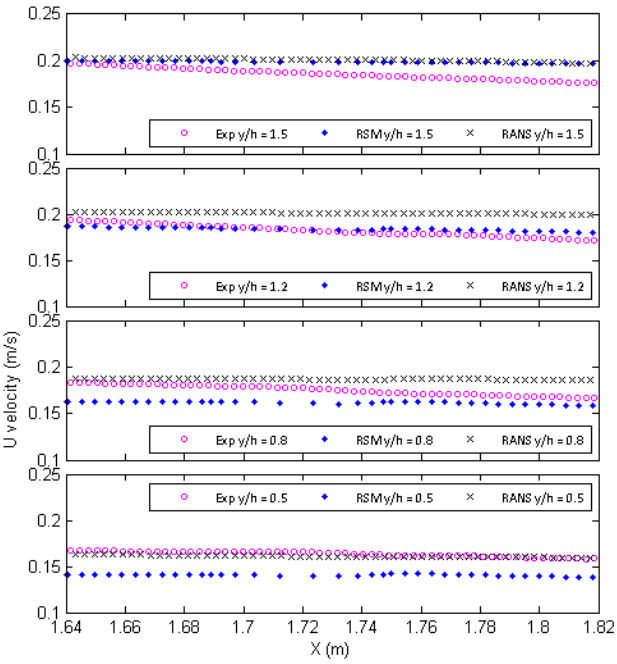

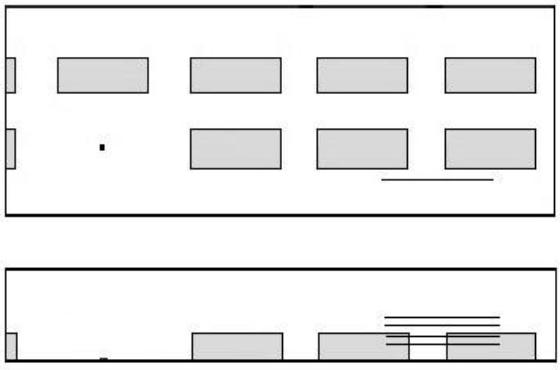

Top and side view of tunnel. Lines indicates the location of the plot on the left.

Figure U4: U velocity at z = 0.104

Appendix A2: V velocity plots at different x and z locations

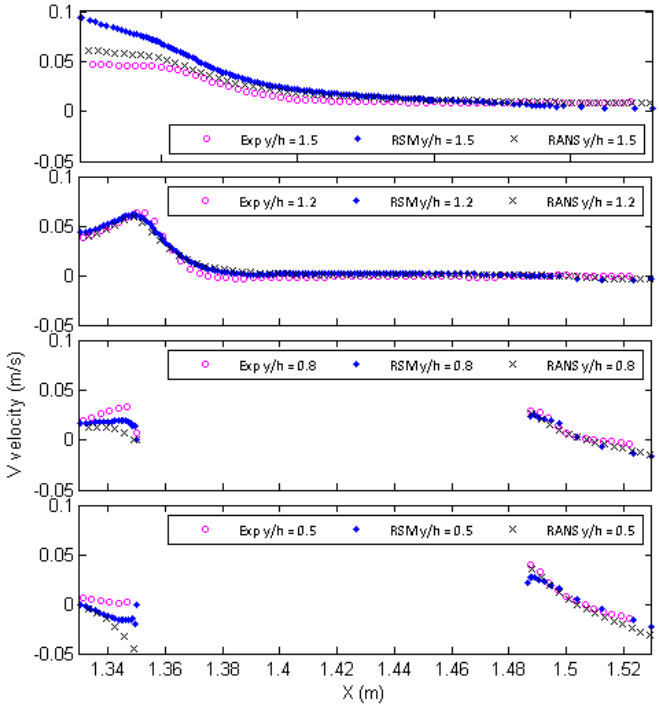

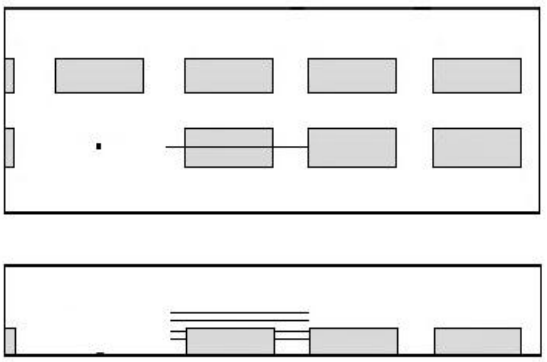

Top and side view of tunnel. Lines indicates the location of the plot on the left.

Figure V1: V velocity at z = 0.056 m

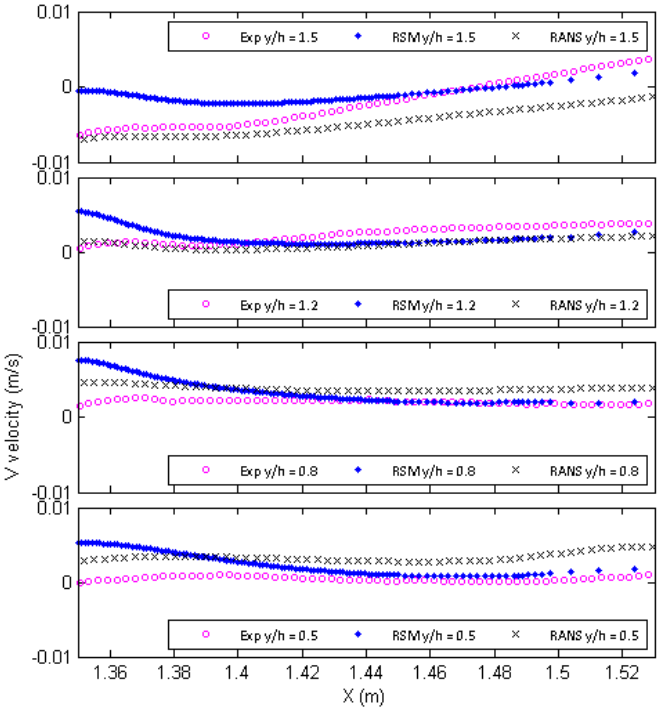

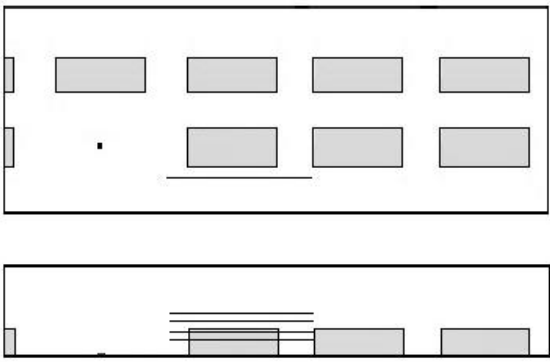

Top and side view of tunnel. Lines indicates the location of the plot on the left.

Figure V2: V velocity at z = 0.104 m

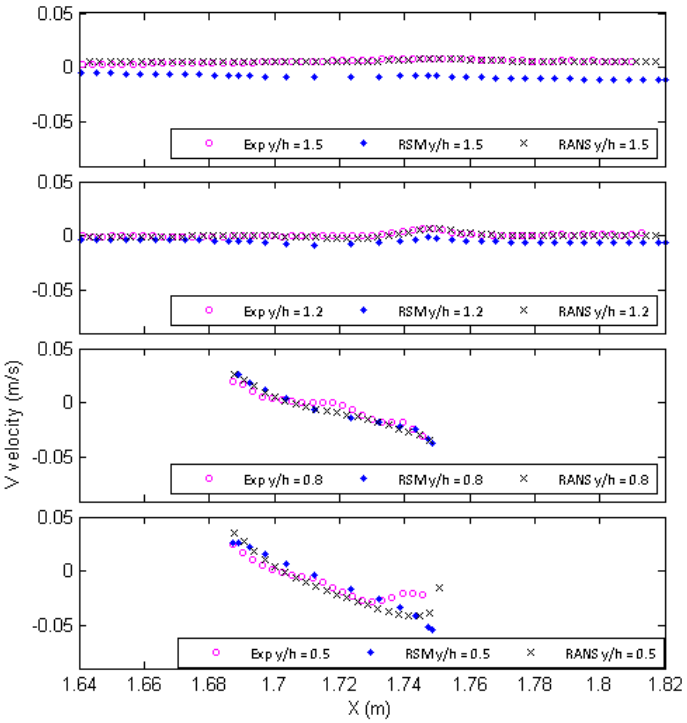

Top and side view of tunnel. Lines indicates the location of the plot on the left.

Figure V3: V velocity at z = 0.056 m

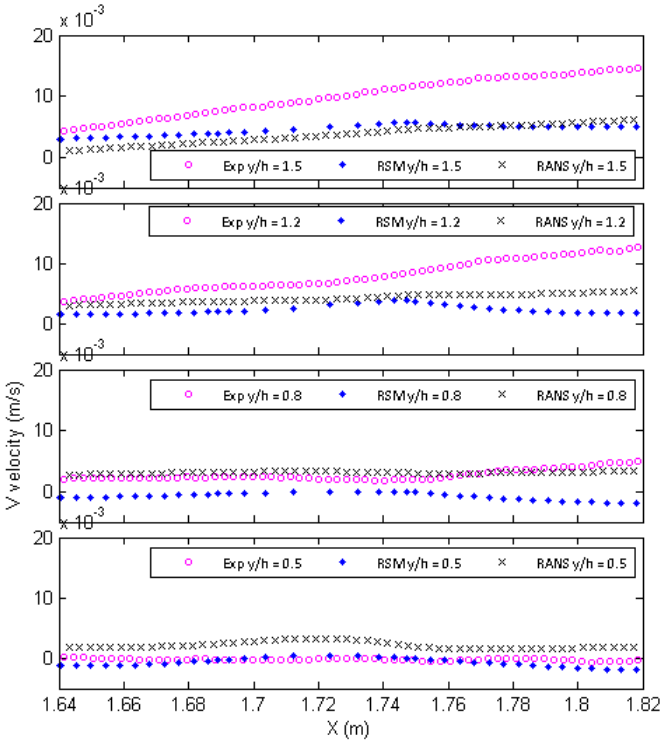

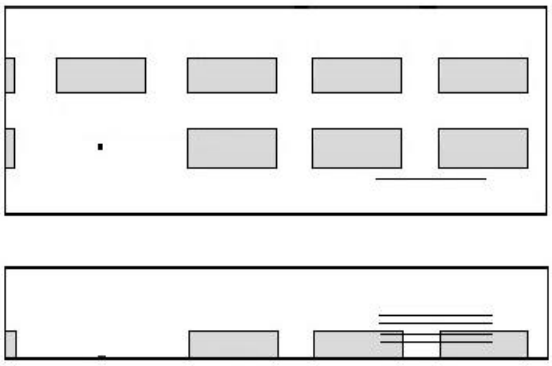

Top and side view of tunnel. Lines indicates the location of the plot on the left.

Figure V4: V velocity at z = 0.104 m

Appendix A3: k, Turbulent kinetic energy (m^2/s^2) at different x and z locations

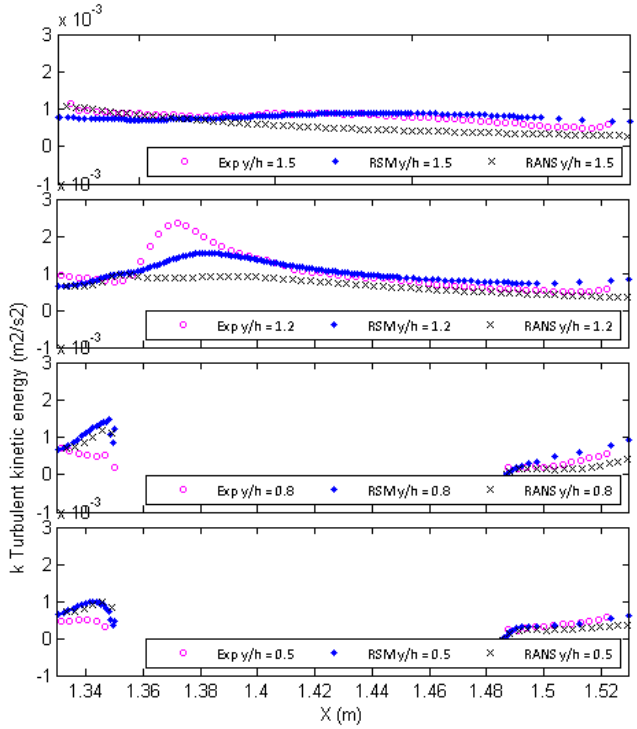

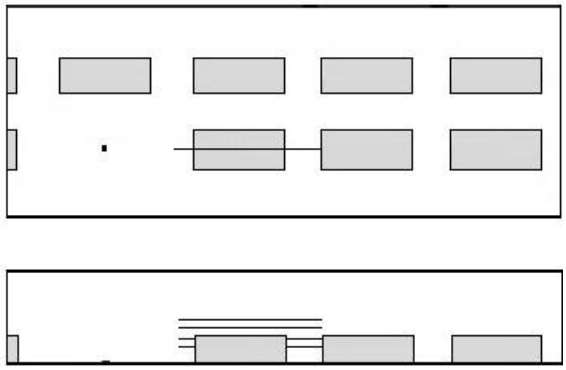

Top and side view of tunnel. Lines indicates the location of the plot on the left.

Figure K1: Turbulent kinetic energy at z = 0.056 m

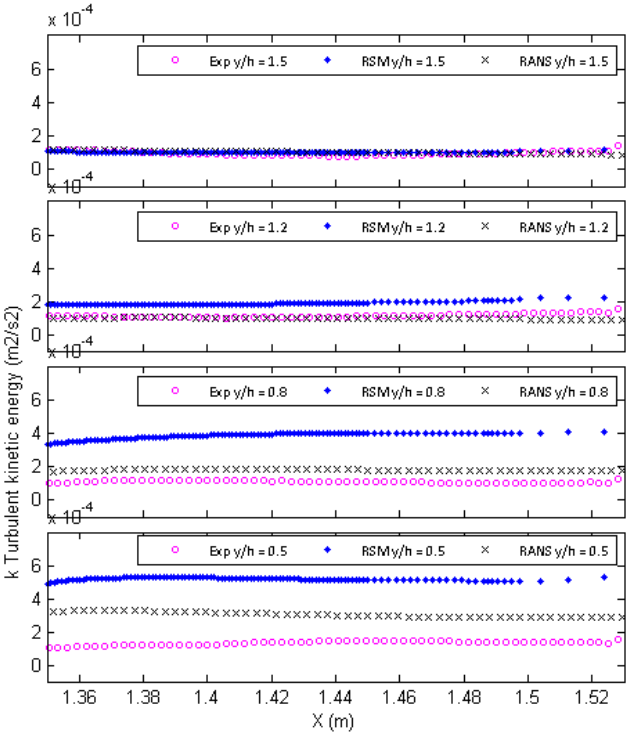

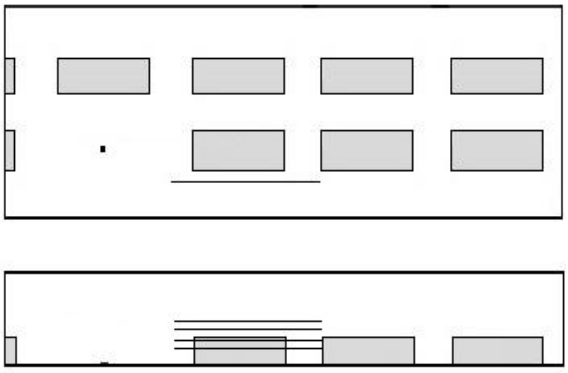

Top and side view of tunnel. Lines indicates the location of the plot on the left.

Figure K2: Turbulent kinetic energy at z = 0.104 m

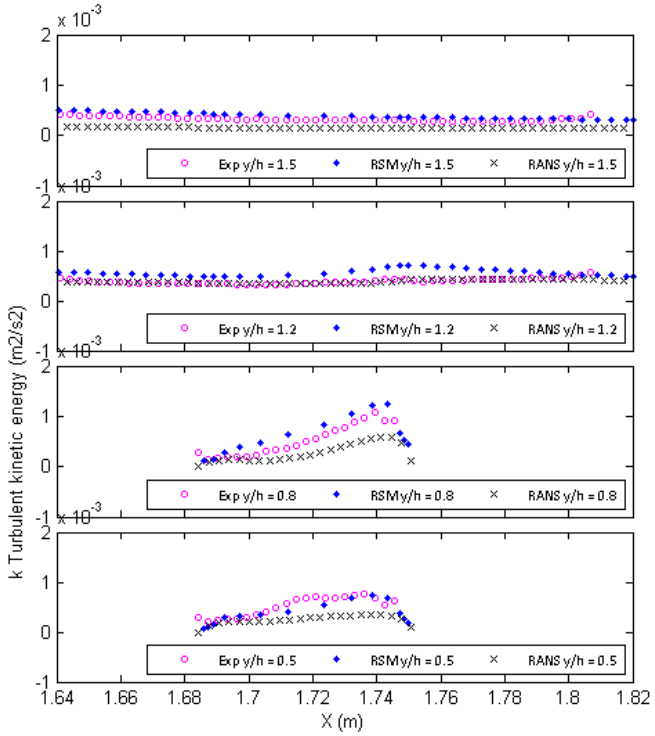

Top and side view of tunnel. Lines indicates the location of the plot on the left.

Figure K3: Turbulent kinetic energy at z = 0.056 m

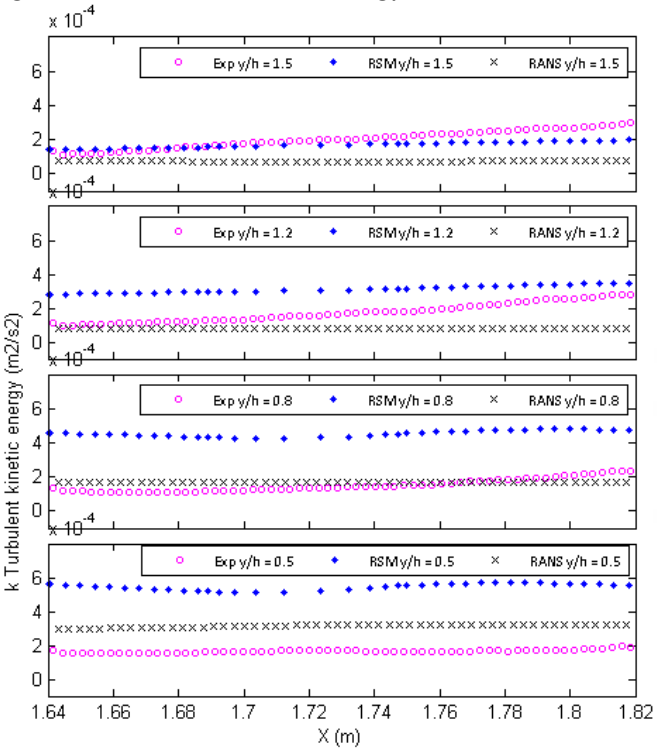

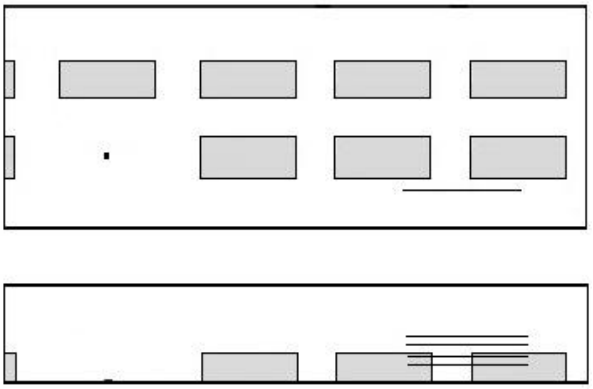

Top and side view of tunnel. Lines indicates the location of the plot on the left.

Figure K4: Turbulent kinetic energy at z = 0.104 m

Appendix A4: *uv* Reynolds stress (m^2/s^2) plots at different x and z locations

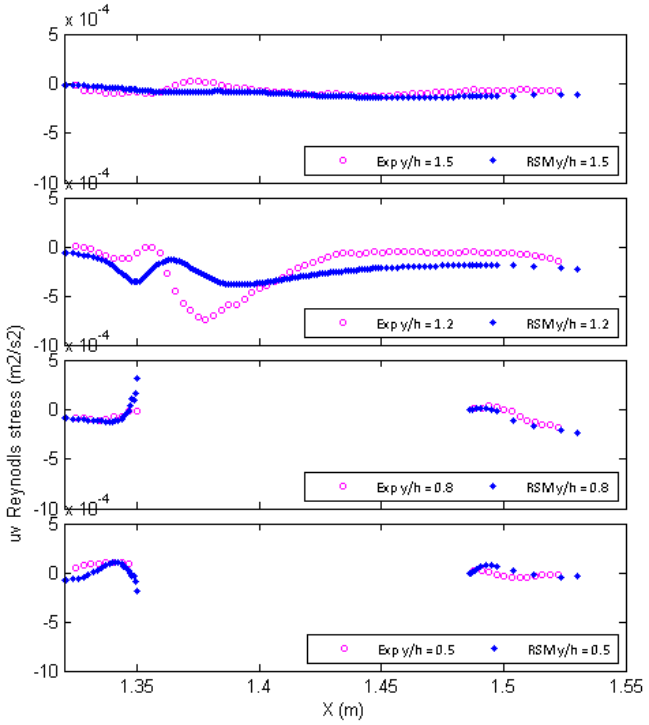

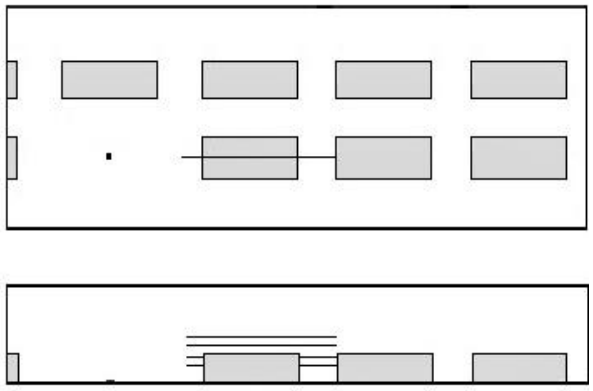

Top and side view of tunnel. Lines indicates the location of the plot on the left.

Figure R1: uv Reynolds stress at z = 0.104 m

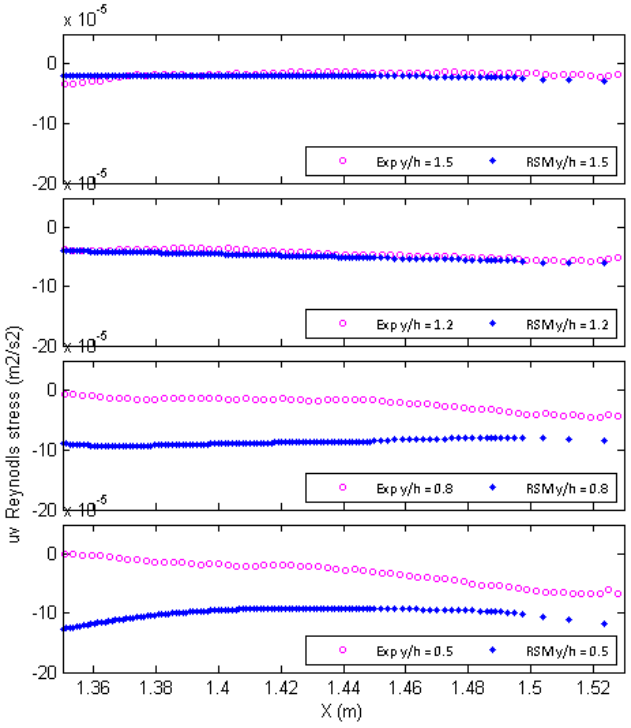

Top and side view of tunnel. Lines indicates the location of the plot on the left.

Figure R2: uv Reynolds stress at z = 0.104 m

Appendix B: Figures

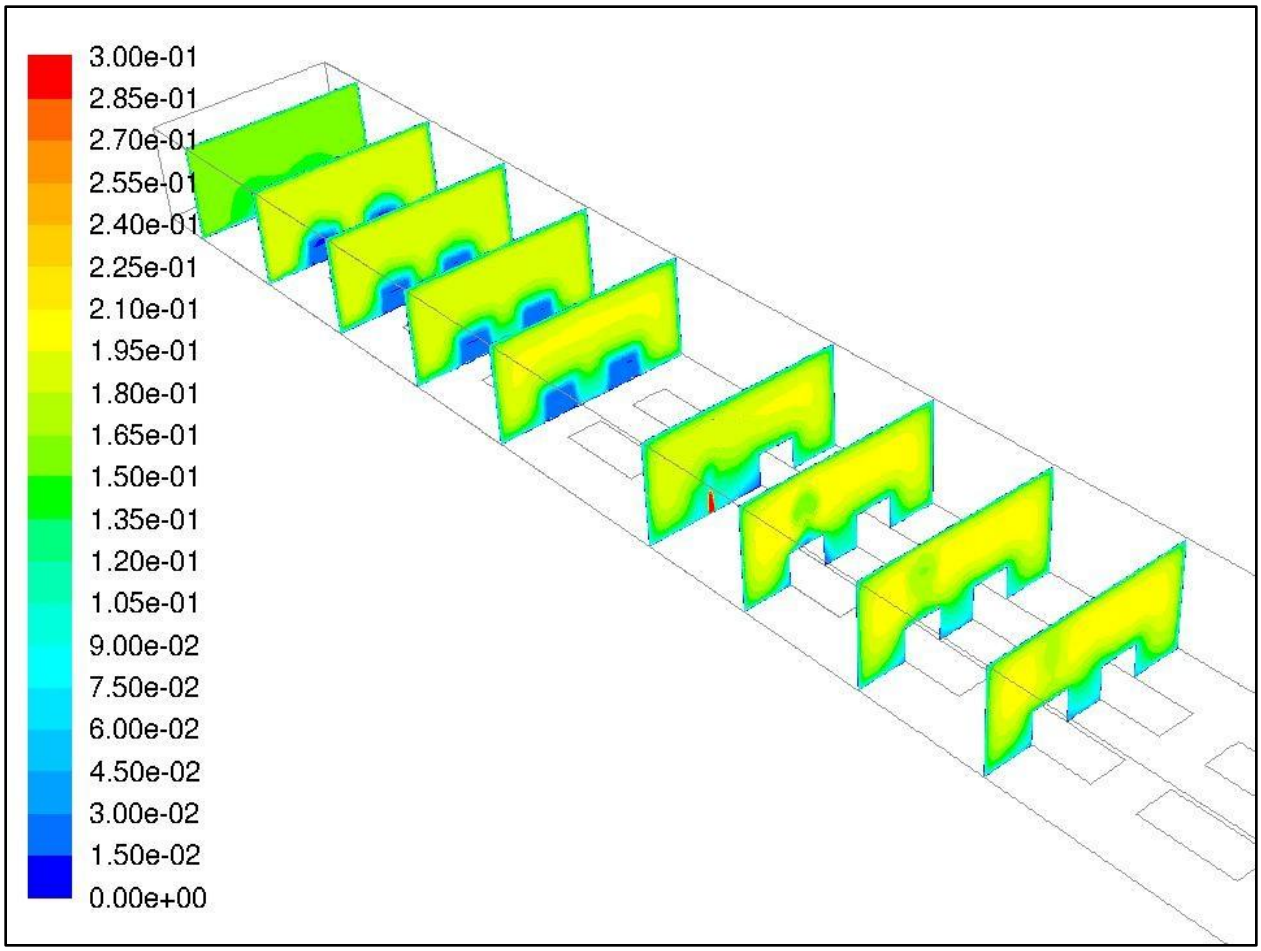

Figure B1: Velocity contour at different location throughout the tunnel

Contour plot before density implementation

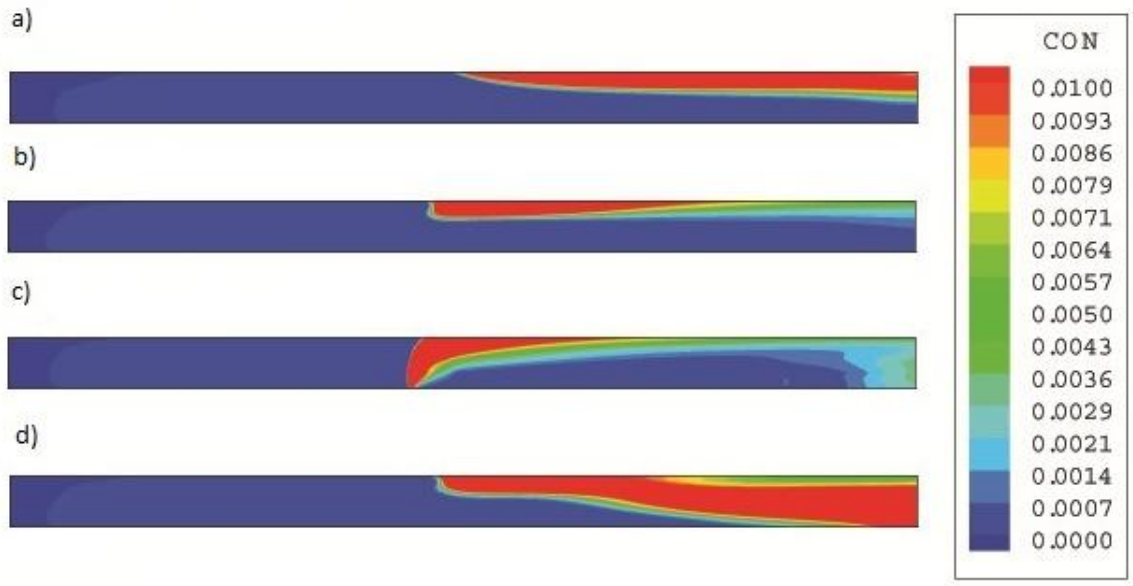

Figure B2: Concentration Contour at, a) z = -0.056m, b) z = 0, c) z = 0.056m, d) z = 0.104m

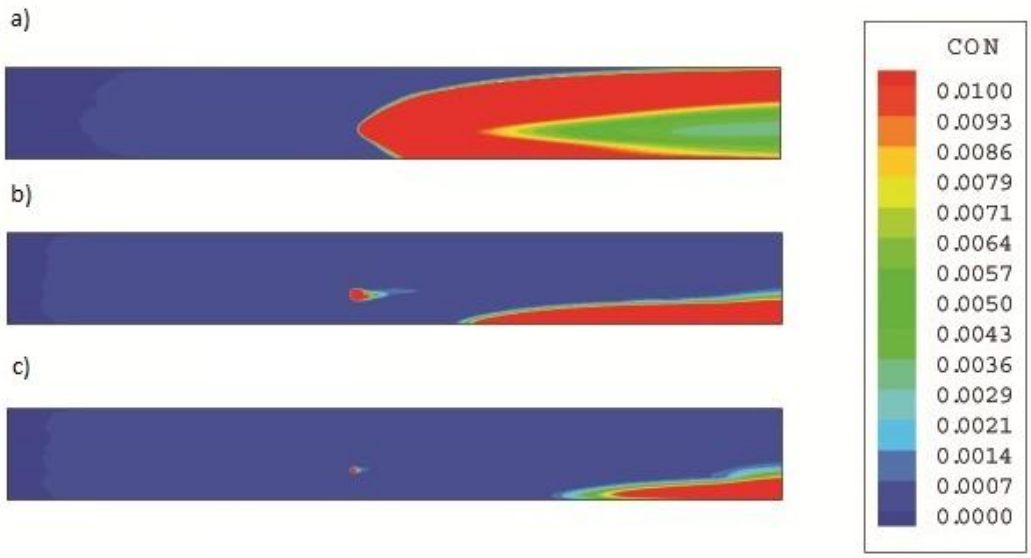

Figure B3: Concentration Contour at, a) y = 0.0245m, b) y = 0.0735m, c) y = 0.14m

Contour plot before density implementation

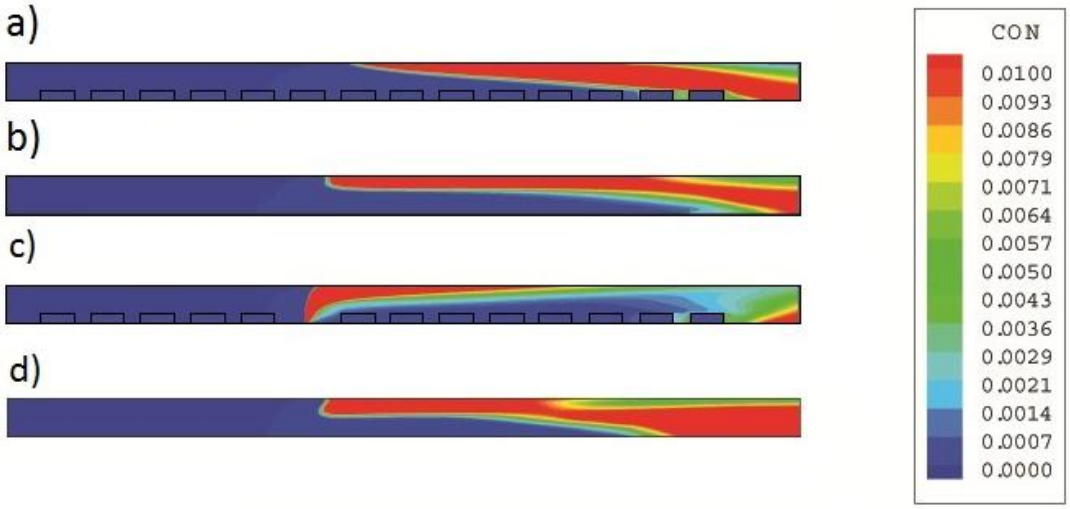

Figure B4: Concentration Contour at, a) z = -0.056m, b) z = 0, c) z = 0.056m, d) z = 0.104m

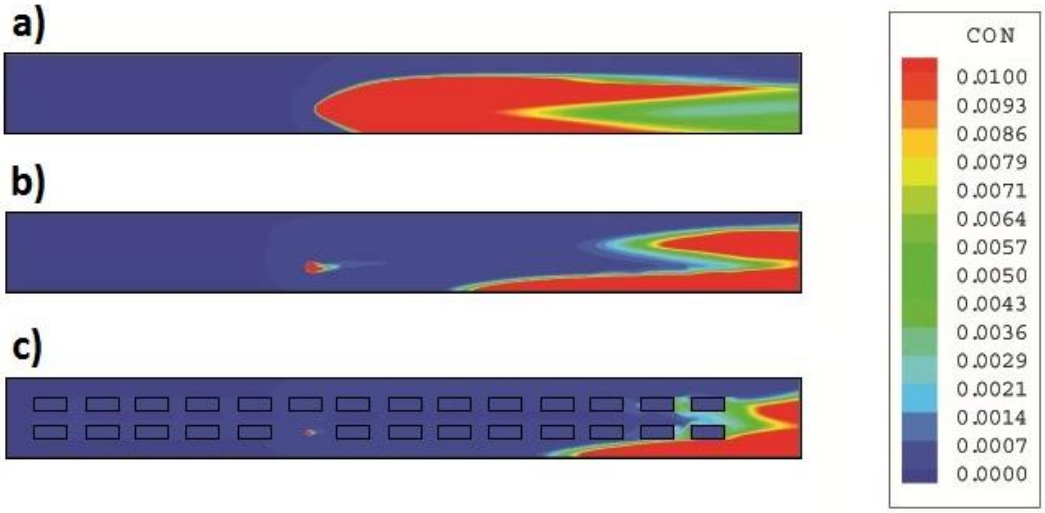

Figure B5: Concentration Contour at, a) y = 0.0245m, b) y = 0.0735m, c) y = 0.14m

Flammable region

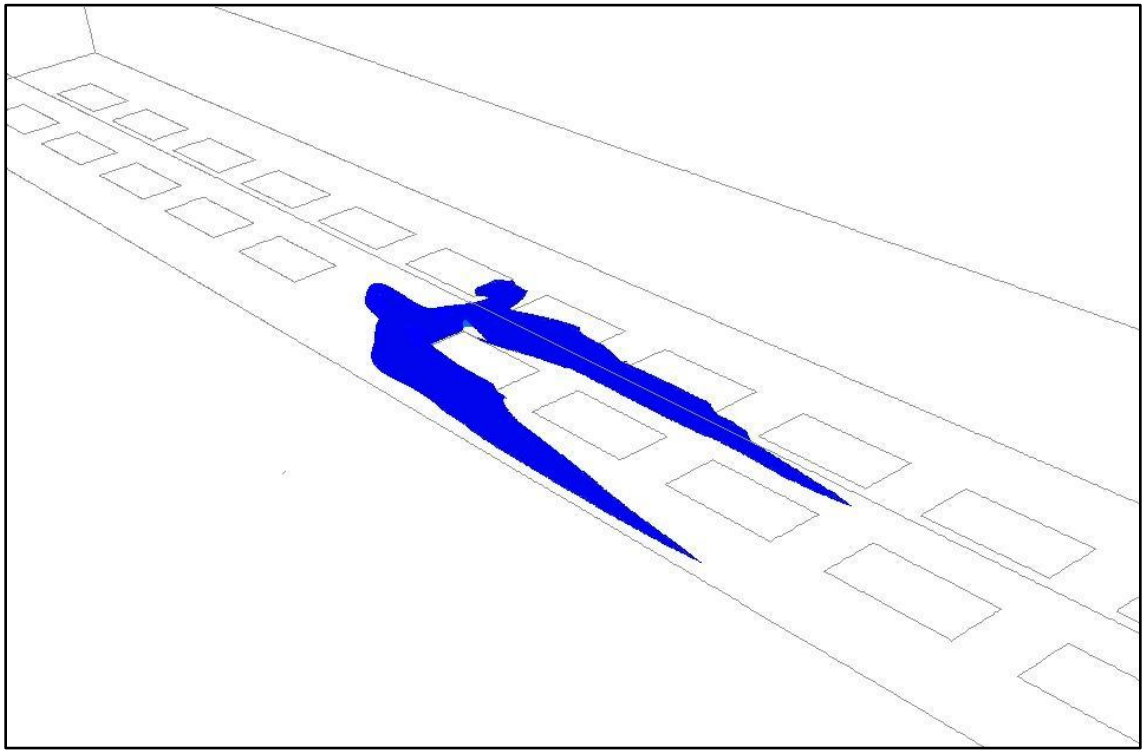

Figure B6: Iso surface of scalar volume percentage at LFL for low jet velocity case

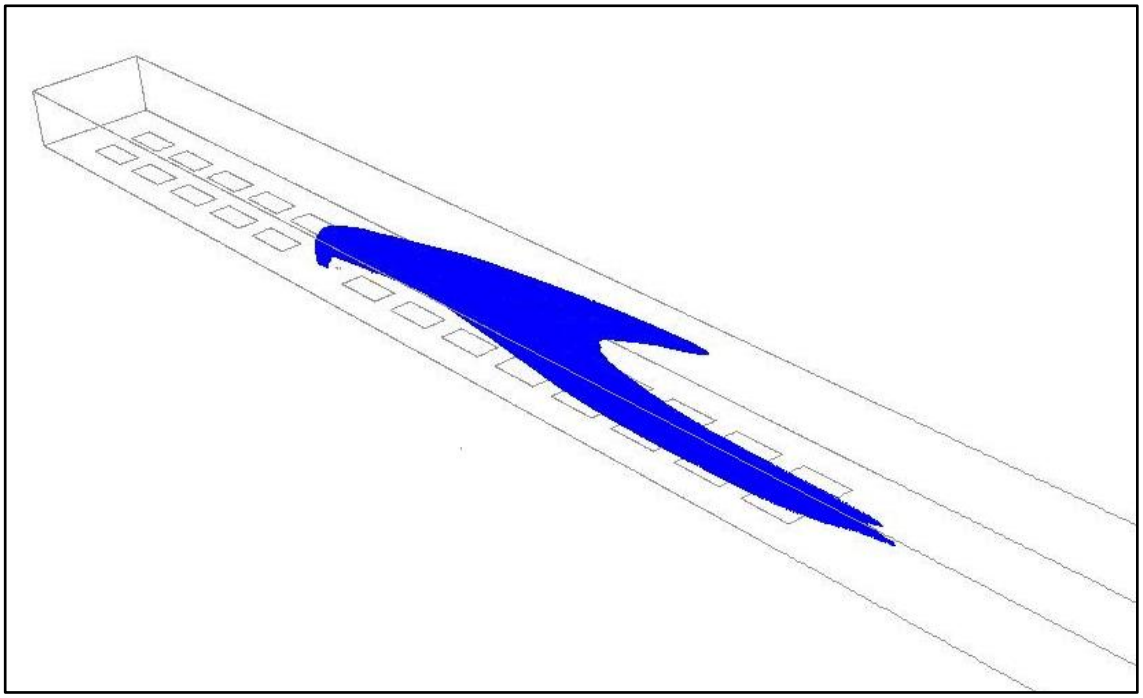

Figure B7: Iso surface of scalar volume percentage at LFL for Hydrogen case

Appendix C: Top and side view of tunnel

Figure C1: Tunnel top view

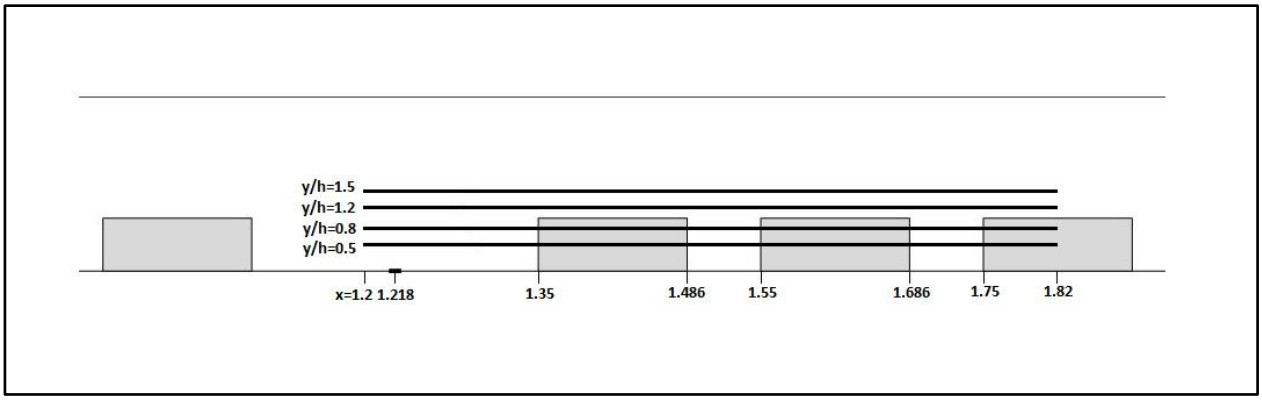

Figure C2: Tunnel side view

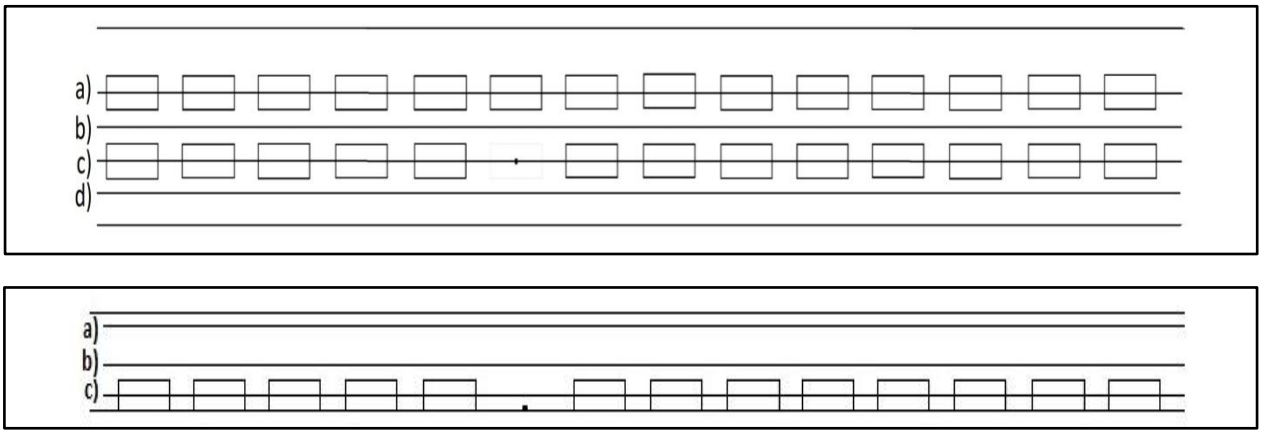

Figure C3: Top and side view of tunnel shows the location of scalar concentration contours

Appendix D: Different Density implementation code

```
C=============================================

DENSIT0=998.

DENSIT1=1060.

DEN(IJK)=DENSIT0*(1-CON(IJK))+DENSIT1*CON(IJK)

C=============================================

SU(INP)=SU(INP)+GRAVX*DEN(INP)*VOL(INP)

SV(INP)=SV(INP)+GRAVY*DEN(INP)*VOL(INP)

SW(INP)=SW(INP)+GRAVZ*DEN(INP)*VOL(INP)

C=============================================
```

Appendix E: Configuration file

```
title: Urban simulation

properties:
  velocity: 0.15
  angle: 0
  density: 998
  viscosity: 0.001003
  pressure: 0
  temperature: 25

  #initial turbulence properties
  turbulence intensity: 5
  viscosity fraction: 62.4

simulation:
  number of presimulations: 0
  do final simulation: [uds, stop, record, quds, record, quds_durbin,
record]
  simulation status: uds

  number of iterations: 10000
  iterations convergence: 1.0e-4
  iterations written every: 3000

  # Reynolds stress model. Options: standard (eddy viscosity), asm
(Algebraic stress model)
  reynolds stress model: standard

  use generalized gradient diffusion hypothesis: false

  constants:
    Cmu: 0.09
    E smooth wall: 8.432
    E rough wall: 30
    C1: 1.44
    C2: 1.92
    von Karman constant: 0.41
    # Cphi for concentration GGDH or AFM
    Cphi: 0.15
    # Ctheta for concentration AFM (SKSI in simulation definition is
1.0-Ctheta)
    Ctheta: 0.4

  #now the numerical properties
  relaxation:
    velocity: 0.6
    pressure: 0.1
    turbulent kinetic energy: 0.6
    energy dissipation: 0.6
    viscosity: 0.8
```

```
    concentration: 0.8
    concentration variance: 0.7
    temperature: 0.8
    temperature variance: 0.7

  time dependent:
    time step: 1.0e10
    number of timesteps: 1
    time iterations: 102
    monitoring points:
      - {x: 1.268, y: 0.028, z: 0.0735}
      - {x: 1.368, y: 0.028, z: 0.0735}

  algebraic stress model:
    constant1: 1.8
    constant2: 0.6
    constant3: 0.6

  cells before end for outlet plane: 3

mesh:
  # Dimensions, setting these to dynamic will make these dynamic based
on obstacles
  # if value is given, space after obstacles is ignored
  width: dynamic
  length: dynamic
  height: dynamic

  x space before obstacles: 0.15
  x space after obstacles: 0.3

  y space before obstacles: 0.076
  y space after obstacles: 0.076

  z space before obstacles: 0
  z space after obstacles: 0.111

  # Set this to 0 to use the full refined mesh without making it more
coarse in pre-simulations
  number of cells in the flow direction: 0

  cell expansion factor: 1.12
  max deviation from cell expansion factor: 0.03
  allow obstacle shifting: false
  required number of cells between obstacles: 0

  scale height to: false

  cell width at walls: 0.0015
  cell length at walls: 0.0015
  cell height at walls: 0.002
```

```
  #if there is no wall or obstacles present, these values will become
the cell sizes
  max cell width: 0.04
  max cell length: 0.04
  max cell height: 0.04

  refined boundary types: [wall]

obstacles:
  default roughness: 1.0e-6

  operations:
    - toZero
    #- flipX

trees:
  constants:
    # Svenson
    drag coefficient: 0.1
    beta p: 1.0
    beta d: 0.0
    C4 epsilon: 1.95
    C5 epsilon: 0.0

walls:
  #give here the wall names and assign a roughness of the wall in
meters
  bottom:
    roughness: 1.0e-6
    inlets:
      - xs: 0.01
        xe: 0.02
        ys: 0.132
        ye: 0.142
        velocity_x: 0
        velocity_y: 0
        velocity_z: 2.3
        turbulence intensity: 5
        viscosity fraction: 50
        concentration: 1.0
  top:
    roughness: 1.0e-6
  south:
    roughness: 1.0e-6
  north:
    roughness: 1.0e-6

system:
  f77 compiler: gfortran -w -O
  editor: gedit
  timezone: Europe/Amsterdam
```